Received: 27 August 2023 | Accepted: 9 October 2023

DOI: 10.1002/pca.3300

RESEARCH ARTICLE

Phytochemical Analysis WILEY

A multiplex approach of MS, 1D-, and 2D-NMR metabolomics in plant ontogeny: A case study on *Clusia minor* L. organs (leaf, flower, fruit, and seed)

Clarice Noleto-Dias[1,2] | Mohamed A. Farag[3] | Andrea Porzel[2] | Josean F. Tavares[1] | Ludger A. Wessjohann[2]

[1]Natural and Synthetic Bioactive Products Graduate Program, Federal University of Paraíba, João Pessoa, PB, Brazil

[2]Department of Bioorganic Chemistry, Leibniz Institute of Plant Biochemistry, Halle (Saale), Germany

[3]Pharmacognosy Department, College of Pharmacy, Cairo University, Cairo, Egypt

Correspondence
Mohamed A. Farag, Pharmacognosy Department, College of Pharmacy, Cairo University, Cairo, 11562, Egypt.
Email: mohamed.farag@pharma.cu.edu.eg

Ludger A. Wessjohann, Department of Bioorganic Chemistry, Leibniz Institute of Plant Biochemistry, Halle (Saale), 06120, Germany.
Email: wessjohann@ipb-halle.de

Present address
Clarice Noleto-Dias, Plant Sciences and the Bioeconomy, Rothamsted Research, West Common, Harpenden, Hertfordshire, UK.

Funding information
Alexander von Humboldt-Stiftung; Ciência sem Fronteiras, Grant/Award Number: SWE-203416/2014-7

Abstract

Introduction: The genus *Clusia* L. is mostly recognised for the production of prenylated benzophenones and tocotrienol derivatives.

Objectives: The objective of this study was to map metabolome variation within *Clusia minor* organs at different developmental stages.

Material and Methods: In total 15 organs/stages (leaf, flower, fruit, and seed) were analysed by UPLC-MS and ^{1}H- and heteronuclear multiple-bond correlation (HMBC)-NMR-based metabolomics.

Results: This work led to the assignment of 46 metabolites, belonging to organic acids(1), sugars(2) phenolic acids(1), flavonoids(3) prenylated xanthones(1) benzophenones(4) and tocotrienols(2). Multivariate data analyses explained the variability and classification of samples, highlighting chemical markers that discriminate each organ/stage. Leaves were found to be rich in 5-hydroxy-8-methyltocotrienol (8.5 μg/mg f.w.), while flowers were abundant in the polyprenylated benzophenone nemorosone with maximum level detected in the fully mature flower bud (43 μg/mg f.w.). Nemorosone and 5-hydroxy tocotrienoloic acid were isolated from FL6 for full structural characterisation. This is the first report of the NMR assignments of 5-hydroxy tocotrienoloic acid, and its maximum level was detected in the mature fruit at 50 μg/mg f.w. Seeds as typical storage organ were rich in sugars and omega-6 fatty acids.

Conclusion: To the best of our knowledge, this is the first report on a comparative 1D-/2D-NMR approach to assess compositional differences in ontogeny studies compared with LC-MS exemplified by *Clusia* organs. Results derived from this study provide better understanding of the stages at which maximal production of natural compounds occur and elucidate in which developmental stages the enzymes responsible for the production of such metabolites are preferentially expressed.

KEYWORDS
2D-NMR metabolomics, Clusiaceae, HMBC, ontogenic changes, prenylated benzophenones, tocotrienols

1 | INTRODUCTION

Holistic and untargeted analyses of plant extracts demand the application of analytical technologies that provide rich qualitative and quantitative information, such as ultrahigh-performance liquid chromatography coupled to mass spectrometry (UPLC-MS) and nuclear magnetic resonance spectroscopy (1D-NMR). Compared with 1D-NMR that can suffer from overlapping signals hindering identification and quantification, 2D-NMR experiments can provide unequivocal or at least much better structural assignments to identify or determine unknown structures which are hard or mostly impossible to assign using MS-based techniques only. Among the 2D-NMR techniques, heteronuclear multiple-bond correlation (HMBC) provides a large number of well-defined signals that provide rich qualitative structural information by the long-range couplings between carbons and protons. Such a technique aided in the identification of novel phloroglucinols in hypericum extract, presenting a potential tool for characterisation of crude plant extracts among omics tools.[1] Although NMR and MS can both provide the same results in principal component analysis (PCA) of discriminatory fingerprints,[2] they are by no means comparable in their potential to elucidate single compounds or classes, especially considering their different detection principles and sensitivity levels.

Clusiaceae Lindl. is a family that belongs to the order Malpighiales[3] that is represented by 15 genera and ca. 800 species. The neotropical genus *Clusia* L. is the largest genus of this family, with 321 species, distributed in Central and South America, from the Bahamas to southern Brazil. *Clusia* species are known to produce a hydrophobic resin from their flowers, a characteristic feature for the attraction of bees that collect it for building nests to prevent against nest insect attack.[4,5]

Phytochemical studies of several *Clusia* species revealed its richness in secondary metabolites, especially prenylated benzophenones and xanthones, proanthocyanidins, terpenes, and tocotrienols, groups associated with many potential biological activities.[6] Benzophenones in *Clusia* show an extraordinary rich prenylation pattern with low oxidation indices.[7] The polyprenylated benzophenones clusianone, chamone I, xanthochymol, and nemorosone exhibit antibacterial,[8] HIV-inhibitory,[9,10] antiplasmodial,[11] and cytotoxic activities.[12,13] Nemorosone and 7-epi-nemorosone are active against breast and prostate carcinoma cell lines, respectively,[14,15] whereas clusiaxanthone and *Z*-δ-tocotrienoloic acid, metabolites of other classes, were isolated from *Chicosciencea pernambucensis* G. Mariz stem bark and showed anti-*Leishmania* properties.[16] Most of these compounds found in *Clusia* contain isoprenoid groups attached to an (originally) aromatic core that play an important role in their pharmacodynamics or pharmacokinetics and are of great potential for the discovery of bioactive agents.[17] Prenylated phenolic acids present novel functions such as in *Humulus lupulus* L. (hop) and *Morus alba* L. as cytotoxic and anti-inflammatory agents[18,19] and have yet to be explored in *Clusia*. Thus, *Clusia* is a perfect research target for our interest in both plant lipids collected by bees[20–22] and prenylated aromatics, for example, in Hypericum.[23–25]

Clusia minor is a dioecious species traditionally used to treat pain and inflammation in sores and warts. Extracts from its leaves exhibit antioxidant, anti-inflammatory, and cytotoxic activities based on in vitro and in vivo studies.[26] The antinociceptive potential of *C. minor* extract was confirmed in a model to assess inflammatory hyperalgesia in mice. The analgesic action was achieved in a dose-dependent manner probably through peripheral and central pathways that modulate pain.[27] Identification of active agents in *C. minor* to account for its effects and for quality control purposes has yet to be reported, especially using advanced analytical tools targeting its whole metabolome.

Previous phytochemical studies of *C. minor* are rather limited especially using omics approaches. Its flower resin was analysed using HPLC, revealing the presence of nine compounds, of which only three peaks were identified as prenylated phloroglucinols based on their MS fragmentation pattern.[28] In another study, three polyprenylated benzophenones derivatives (propolone D, hyperibone B, and garcinielliptone I, all m/z 519 $[M + H]^+$), were isolated from its fruits.[29] More recent studies focused on the GC-MS analysis of its leaves, with the detection of sterols, triterpenes, volatiles, and vitamin E.[26,27]

With an increasing interest in the *Clusia* genus' health benefits and the lack of detailed phytochemical studies of its species to justify such applications scientifically, and also to evaluate other potential uses based on its rich constituents, the objective of the present work was to assess the metabolome variation of *C. minor* organs at different developmental stages via UPLC-MS and NMR fingerprinting. One successful application of HMBC in *H. lupulus* (hops) resin classification from different cultivars coupled to multivariate data analysis such as PCA has been reported by our group,[30] which we extend herein for the assessment of ontogenic effects in *Clusia* for its different organs including leaf, flower, fruit, and seed. Results derived from this study provide better insights into the biosynthetic pathways regulating the production of *Clusia* metabolites. It also can reveal the best harvesting stages of natural compounds of interest and offers opportunities to identify the enzymes and genes involved in their generation, for example, by parallel transcriptomics.

2 | EXPERIMENTAL

2.1 | Chemicals

Methanol-d4 (99.80% D), acetone-d6 (99.80% D), and hexamethyldisiloxane (HMDS) were purchased from Deutero GmbH (Kastellaun,

Germany). For NMR quantification and calibration of chemical shifts, HMDS was added to a final concentration of 0.935mM. Acetonitrile, methanol, water, and acetic acid (LC-MS Chromasolv grade) were obtained from Fluka Analytical Sigma-Aldrich (Munich, Germany). Chromoband C18 ec (1 mL 100 mg^{-1}) cartridge was purchased from Macherey and Nagel (Düren, Germany). All other chemicals and standards were purchased from Sigma-Aldrich (St. Louis, MO, USA).

2.2 | Plant material

Different developmental stages and organs of *C. minor* shrub grown in a greenhouse facility at the Leibniz Institute of Plant Biochemistry (IPB), Halle, Germany were harvested between June 2015 and April 2016. Plant material was immediately frozen in liquid nitrogen, transported in a box with dry ice and stored at −80°C. Deep-frozen plant material was milled in liquid nitrogen using pestle and mortar. All information on collected samples and their maturity stage is recorded in Table 1 and Figure 1.

2.3 | Metabolites extraction

Each organ sample (150 mg) was extracted in 5 mL 100% methanol containing 5 µg/mL umbelliferone (internal standard) in an ultrasound bath for 15 min. Extracts were then vortexed vigorously and centrifuged at 8000 × *g* for 5 min at 5°C. For UPLC-MS analysis, an aliquot (900µL) was taken and placed on a C18 silica-based cartridge (100 mg) preconditioned with methanol and water. Samples were then eluted with 900 µL MeOH into an autosampler glass vial. For NMR analysis, 3.5 mL extract was transferred to a glass vial and dried under a gentle stream of nitrogen. Pellets were then resuspended in 800 µL methanol-d4 containing HMDS (0.935mM) (internal standard). After centrifugation (13,000 × *g* for 1 min), the supernatant was transferred to a 5-mm NMR tube. Each developmental stage/organ had two biological replicates and one technical replicate for each one of the biological replicates. The extraction procedure was performed under minimal light condition and at low temperatures (transported in dry ice) to prevent against metabolite decomposition.

TABLE 1 Codes for the different developmental stages and organs of *Clusia minor* L. analysed in this work.

Codes	Stage/organ
L1	Expanding leaves
L2	Mature leaves
FL1	Juvenile bud stage
FL2	Second green bud stage
FL3	Third green bud stage
FL4	Fourth green bud stage
FL5	First pink bud stage
FL6	Fully mature bud
FL7	Preanthesis flower stage
FL8	Fully open flower
FL9	Senescent flower
FR1	Immature fruit
FR2	Mature fruit
FR3	Fully expanded fruit
SE	Seeds of expanded fruit

2.4 | UHPLC-HRMS analysis

LC-MS was recorded on an Orbitrap Elite mass spectrometer (Thermo Fisher Scientific, Germany) coupled to a Dionex UltiMate 3000 UHPLC system and equipped with a DAD-3000 photodiode array detector. Samples were injected (2 µL) onto a RP-18 column (particle size 1.9 µm, pore size 175 Å, 50 × 2.1 mm ID, Hypersil GOLD, Thermo Fisher Scientific) maintained at 40°C. The solvent system consisted of water/0.1% formic acid (A) and acetonitrile/0.2% formic acid (B). Total run time was 15 min using a flow rate of 0.4 mL/min and the following elution gradient: 0–1 min, isocratic 5% B; 1–1.5 min, 70% B; 1.5–8.5 min, 100% B; 8.5–10 min, isocratic 100% B; and 10–15 min, isocratic 5% B. Mass spectra were acquired in negative ion mode with a heated electrospray ionization (ESI) source at 400°C, spray voltage 3.0 kV, capillary temperature 300°C, FTMS resolution 30,000, and sheath and auxiliary gas (nitrogen) at 30 (arbitrary units) and 15 (arbitrary units), respectively. Collision-induced dissociation (CID) mass spectra (buffer gas: helium) were recorded using normalised collision energy of 35%. The instrument was externally calibrated by the Pierce ESI negative ion calibration solution (product No. 88324) from Thermo Fisher Scientific. Data were inspected using Xcalibur v. 2.2 SP1.48 (Thermo Fisher Scientific, Germany).

2.5 | NMR spectroscopy analysis

All spectra were recorded on a Varian/Agilent VNMRS 600 NMR spectrometer operating at proton and carbon NMR frequencies of 599.83 and 150.84 MHz, respectively using a 5-mm inverse detection cryoprobe. ^{1}H-NMR spectra were recorded using a spectral resolution of 0.26 Hz/point [SW = 8389 Hz, acquisition size = 64 K of complex points, zero filled to a final Fourier transform (FT) size of 128 K]. Other parameters applied: pulse width (pw) = 6 µs (90°), relaxation delay = 22.3 s, acquisition time = 2.7 s, and number of scans = 120. HMBC spectra were collected over a bandwidth of 14 ppm in F2 (^{1}H) and 235 ppm in F1 (^{13}C) using two scans per 256 increments for F1 and 2516 complex data points in F2. HMBC experiments were optimised for long-range couplings of 8 Hz, a 1-s relaxation delay and 0.15-s acquisition time that resulted in a total acquisition time of 22 min. All NMR spectra were acquired within samples prepared immediately before data acquisition (maximum 6 h time interval) to reduce degradation and artefact formation. Spectra were automatically phase adjusted and proton and carbon chemical shifts were

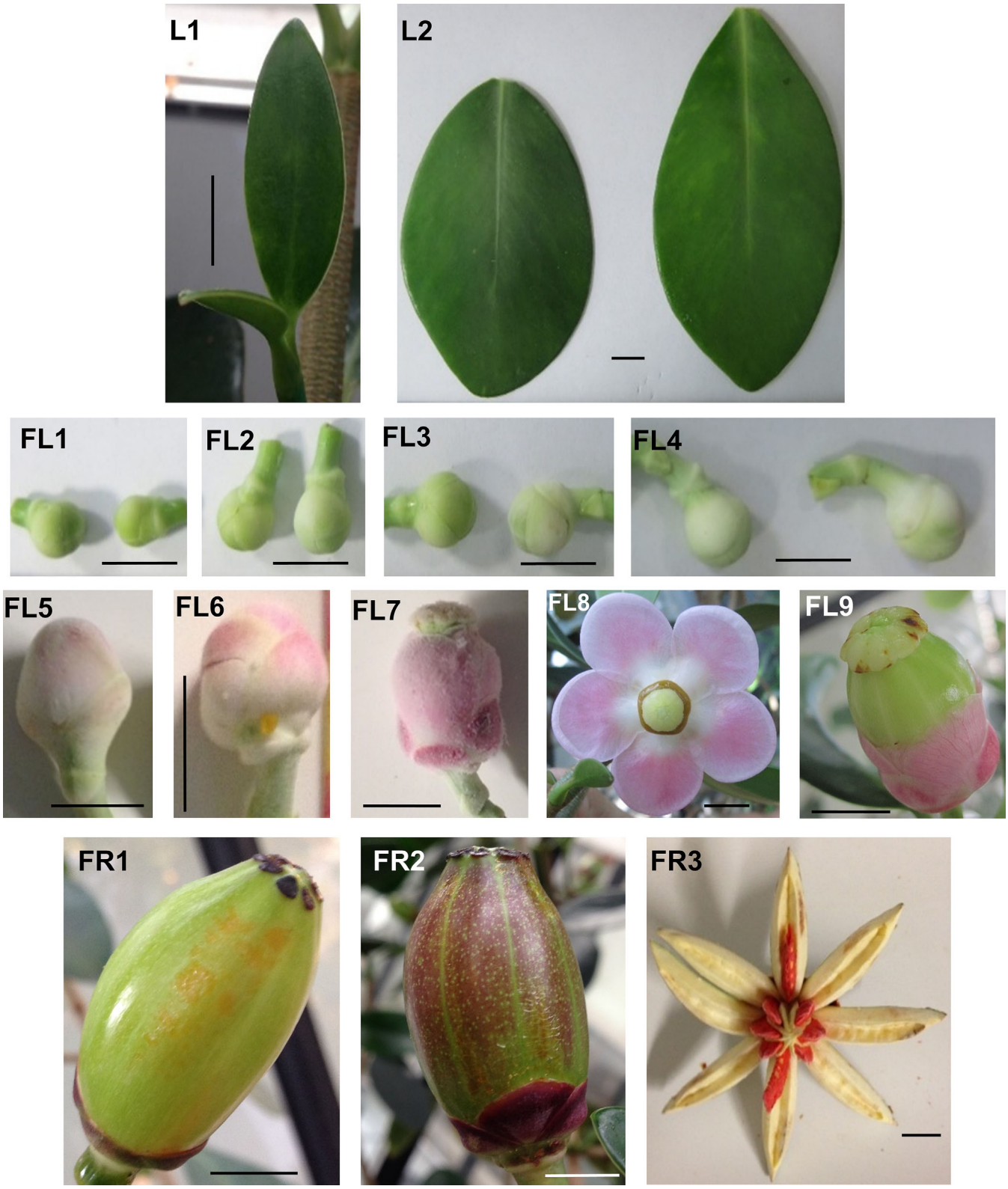

FIGURE 1 Representative photos of *Clusia minor* L. parts at different stages used in this study. Codes refer to Table 1. Scale bars = 1 cm. L1, expanding leaves; L2, mature leaves; FL1, juvenile bud stage; FL2, second green bud stage; FL3, third green bud stage; FL4, forth green bud stage; FL5, first pink bud stage; FL6, fully mature bud; FL7, preanthesis flower stage; FL8, fully open flower; FL9, senescent flower; FR1, immature fruit; FR2, mature fruit; FR3, fully expanded fruit. [Colour figure can be viewed at wileyonlinelibrary.com]

referenced to HMDS (δ $^{1}H = 0.062$ ppm) and internal CD_3OD (δ $^{13}C = 49.0$ ppm), respectively.

Further 2D-NMR spectra were recorded for selected samples, namely ^{1}H–^{1}H correlation spectroscopy (COSY), ^{1}H–^{1}H total correlation spectroscopy (TOCSY), ^{1}H–^{13}C heteronuclear single-quantum coherence (HSQC), and ^{1}H–^{13}C HMBC, using standard CHEMPACK 7.1 pulse sequences (gDCOSY, zTOCSY, gHSQCAD, and gHMBCAD, respectively) implemented in Varian VNMRJ 4.2A spectrometer software.

2.6 | Isolation of major compounds from the flowers

A Shimadzu prominence system (Kyoto, Japan) consisting of an SPD-M20A photodiode array detector, a CBM-20A communication bus module, a DGU-20A5R degassing unit, and an LC-20AT HPLC pump was used for semi-preparative separation of the two major compounds of *C. minor* flowers. A reversed-phase column and a gradient mobile phase of acetonitrile and water was used. Collected fractions were dried under nitrogen stream and the obtained white powder was analysed by UPLC-MS and NMR spectroscopy as described above.

2.7 | UPLC-MS, 1D-, and 2D-NMR data processing for multivariate data analyses

Native UPLC-MS files were converted into mzML. Converted files were analysed in the XCMS package, under R Studio environment for peak detection, alignment, integration, and relative quantification, using custom-written procedures. $^{1}H^{-}$NMR spectra of all samples were stalked using MestReNova version 10.0 software (Mestrelab Research SL, Spain) and preprocessed, with baseline correction (polynomial fit—order 3) and normalisation by scaling to HMDS signal. Spectral intensities were reduced to integrated regions, referred to as buckets, of equal width (0.04 ppm) within the region of δ_H 10.0 to −0.4 ppm. The regions between δ_H 5.0–4.7 and 3.4–3.25 ppm corresponding to residual water and methanol signals, respectively, were removed prior to multivariate analyses.

^{1}H–^{13}C HMBC spectra of all samples were processed using a sine bell window function in F2, zero filling up to 1024 K, and a Gaussian window function in F1 prior to Fourier transformation to ESP files using ACD/NMR Manager lab version 10.0 software (Toronto, Canada). For statistical analysis, spectral intensities were reduced to 2D integrated regions, referred to as pixels, that is rectangles, of constant length and width in the spectral regions δ_C (−5.0 to 230 ppm) in F1 and δ_H (−2 to 12 ppm) in F2 and an intensity value per pixel (i.e. the pixels are the 2D equivalents of the "buckets" in 1D spectra). Pixel sizes were set at 0.925 ppm in the F1 dimension (^{13}C) and 0.04 ppm in the F2 dimension (^{1}H), with the noise factor set to 3. The regions corresponding to residual water and methanol signals were removed prior to analyses. PCA calculated based on 2D-NMR HMBC fingerprint was performed with the open-source statistic software R (2.9.2) together with the Bioconductor package pcaMethods using an R script developed in-house and a normalisation to sum of integral set at 10,000 as previously described.[30]

The resulting integral list from 1D- and 2D-NMR spectra were imported into SIMCA-P 14.1 software package (Umetrics, Umea, Sweden), where the data were subjected to hierarchical cluster analysis (HCA), PCA, and orthogonal projections to latent structures discriminant analysis (OPLS-DA). All variables were mean centred and scaled to Pareto variance. PCA and HCA were run for obtaining a general overview of the variance of metabolites and to identify organ markers.

2.8 | NMR quantification

^{1}H-NMR spectra of all samples were acquired with a sufficient long relaxation delay of 22.3 s, ensuring full relaxation of all proton resonances during signal acquisition. The peak areas of the internal standard signal (HMDS) and of the selected proton signals of the target compounds were integrated using the peak-peaking algorithm for all the samples. In most of the cases, more than one peak was used for standard deviation (SD) calculation. The following equation was applied for calculation:

$$m_T = M_T \times \frac{I_T}{I_{st}} \times \frac{X_{st}}{X_T} \times C_{st} \times V_{st}$$

m_T mass of the target compound in the solution prepared for the ^{1}H-qNMR measurement (μg)

M_T molecular weight of the target compound (g/mol)

I_T relative integral value of the ^{1}H-NMR signal of the target compound

I_{st} relative integral value of the ^{1}H-NMR signal of the internal standard

X_{st} number of protons belonging to the ^{1}H-NMR signal of the internal standard

X_T number of protons equivalent to the ^{1}H-NMR signal of the target compound

C_{st} concentration of internal standard in the solution used for ^{1}H-NMR measurement (mmol/L) corrected to its purity (99%)

V volume of solution used for ^{1}H-NMR measurement (mL)

The results are expressed as mean ± SD of three measurements. Significant differences between the values of the metabolite levels were determined at $p < 0.05$ according to one-way analysis of variance (ANOVA) with Tukey's post hoc test using GraphPad Prism® version 5.0.

3 | RESULTS AND DISCUSSION

The major goal of this study was to assess the metabolite heterogeneity and changes in *C. minor* L., in the context of its different organs

(viz. leaf, flower, fruit, and seed) during development and ripening, in an untargeted and comprehensive manner, using UPLC-MS and NMR-based metabolomics. This study included expanding and mature leaves, nine developmental flowering stages, three fruit samples at different maturation levels, and the seeds from the expanded fruit. The goal of the present study was to assess metabolites biosynthesised by the different organs of *C. minor*, pairing UPLC-MS, and NMR analyses.

The results provide new insights into the secondary metabolism of a representative of the *Clusia* genus and helps to better valorise its potential as source of medicinally or otherwise useful phytoconstituents.

3.1 | Metabolites identified in *C. minor* L. extracts

Metabolites were identified by comparing their UPLC-MS (R_t, UV/Vis spectra and MS data, accurate mass, isotopic distribution, and fragmentation pattern) and NMR features (chemical shifts, coupling constants, and 2D correlations) with those reported in the literature. Searches were carried out in the following databases: Reaxys, SciFinder, and Phytochemical Dictionary Database (CRC, Wiley). MS/MS spectra were submitted to in silico fragmentation in MetFrag (http://msbi.ipb-halle.de/MetFrag/). Identifications were confirmed with authentic standards whenever available commercially or in-house. Such comparative approach of NMR and LC/MS aided the structural elucidation especially for several regioisomers that we failed to confirm using LC/MS only. They required 2D-NMR for proof of structural assignment.

Metabolite profiles obtained by UPLC-MS and ^{1}H-NMR of leaves, flowers, fruits, and seeds of *C. minor* methanol extracts showed significant visual quantitative and qualitative differences. LC-MS base peak chromatograms of the different organs of *C. minor* are presented in Figure 2. UPLC-MS peak assignments are described in Table 2, while detected features that were confirmed using NMR are presented in Table 3. Chemical structures of key metabolites are presented in Figure 3 with compounds identified using UPLC-MS denoted with L versus N in case of NMR.

To the best of our knowledge, 1D- and 2D-NMR experiments have not been previously reported for metabolite fingerprinting of *Clusia* species. A comparative ^{1}H-NMR spectrum of different developmental stages of *C. minor* L. organs is illustrated in Figure S1. The ^{1}H-NMR spectrum of fully mature bud flower (FL6) extract is displayed in more detail in Figure 4A as a representative example of *C. minor* to show relative peak abundance and major classes identified using NMR. Expanded spectral regions are shown in Figure 4B–D, and signal numbers correspond to those listed in Table 3.

The HMBC spectrum of the FL6 extract is displayed in Figure S2 and approximately can be divided into three main regions along the F2 proton dimension. Different classes of metabolites were identified as evident from their characteristic NMR signals described further down in detail. In the region I at δ ^{1}H values between 5 and 8 ppm, signals are well resolved in the extension of mostly the δ ^{13}C values at 100 to 200 ppm of the F1 axis, comprised of prominent moieties such as aromatic rings and olefinic chains in phenolics and prenylated metabolites, a major secondary metabolite class in *Clusia*. The second region (II) of the HMBC spectrum includes mainly cross peaks along the F1 dimension at δ ^{13}C 40–80 ppm, in which signals correspond to sugars. The strongest cross peaks are in the third region (III) at δ ^{1}H of 0.5–3.5 ppm and are spread along the full length of the F1 carbon dimension (δ ^{13}C 10–210 ppm) ascribed to methylene and methyl groups of prenylated metabolites, the most characteristic natural product class of *Clusia*,[9] accounting for most of its described biological effects.

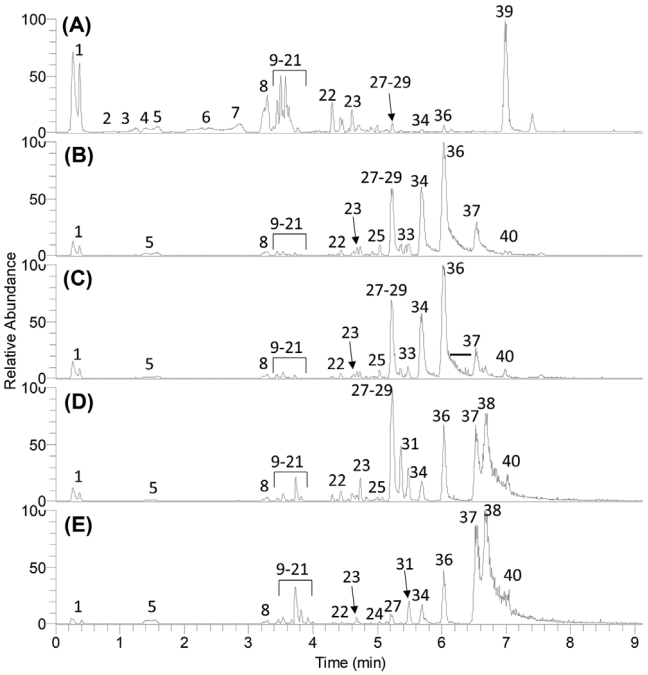

FIGURE 2 UPLC-MS-based chromatograms of different organs of *Clusia minor* L. methanol extracts, measured in negative ionisation mode: expanding leaves L1 (A), fully mature bud flower FL6 (B), fully open flower FL8 (C), mature fruit FR2 (D), and seeds SE (E). Chromatographic conditions are described in the experimental section. The identities, retention times, and basic UV and MS data of all peaks are listed in Table 2.

A total of 46 metabolites were annotated combining the analysis of UPLC-MS and NMR datasets. Metabolites belonged to organic acids, fatty acids, phenolics, flavonoids, xanthones, benzophenones, and tocotrienols.

Some common plant metabolites were readily assigned by NMR. Signals in the upfield region, namely at δ_H 2.32 ppm (J = 7.8 Hz) and 1.62 ppm, were of fatty acids (**N1**), and these were present almost exclusively in seeds as typical storage organ of the plant (Figure S1). Linoleic acid (**N2**), an omega-6 fatty acid enhanced in the seeds, was identified from the three signals at δ_H 5.33, 2.77 and 0.90 ppm, corresponding to methine, methylene, and terminal methyl groups, respectively (Figure S3), and suggestive that omega-6 fatty acid is enriched in *C. minor* seed. On the other hand, two doublets at δ_H 2.90 and 2.78 ppm (J = 15.5 Hz, H-3), only detected in the leaves, were assigned to citric acid (**N3**). This is further confirmed from key HMBC

TABLE 2 Peak assignments in *Clusia minor* L. methanol extracts via UPLC-MS in negative ionization mode.

Peak no.	$[M-H]^-$ (*m/z*)	Rt (min)	UV (nm)	Molecular formula	Error (ppm)	MS/MS product ions (*m/z*)	Identification	Metabolite class
L1	191.0196	0.37	281, 351, 369	$C_6H_8O_7$	−0.55	67.0195, 87.0089, 111.0088, 129.0193, 147.0302, 154.9987, 173.009	Citric acid* (N3)	Organic acid
L2	353.0875	0.90	297, 323, 390	$C_{16}H_{18}O_9$	−0.79	179.0348, 191.0561	Caffeoylquinic acid isomer	Phenolic acid
L3	577.1342	1.24	281, 361	$C_{30}H_{26}O_{12}$	−1.72	245.0808, 273.0384, 287.0553, 289.0711, 299.0552, 331.08, 381.0951, 407.0758, 425.0863, 433.0942, 451.102	B-type proanthocyanidin	Flavanol
L4	337.0926	1.46	280	$C_{16}H_{18}O_8$	−0.98	119.0468, 163.0406, 191.0566	*p*-Coumaroylquinic acid (N8)	Phenolic acid
L5	289.0715	1.55	280	$C_{15}H_{14}O_6$	−1.00	125.0242, 135.0079, 167.0338, 179.0342, 203.0713, 205.0499, 231.0292, 245.0812	Catechin* (N10)	Flavanol
L6	353.0874	2.25	280, 326, 390	$C_{16}H_{18}O_9$	−1.23	135.0439, 173.0453, 179.0348, 191.055	Chlorogenic acid* (N9)	Phenolic acid
L7	577.1343	2.82	280, 340	$C_{30}H_{26}O_{12}$	−1.51	245.0808, 273.0384, 287.0553, 289.0711, 299.0552, 331.08, 381.0951, 407.0758, 425.0863, 433.0942, 451.102	Procyanidin B2*	Flavanol
L8	289.0714	3.29	280	$C_{15}H_{14}O_6$	−1.10	125.0242, 135.0079, 167.0338, 179.0342, 203.0713, 205.0499, 231.0292, 245.0812	Epicatechin* (N11)	Flavanol
L9	865.1962	3.45	210, 313	$C_{45}H_{38}O_{18}$	+1.32	289.0712, 407.0758, 413.0858, 425.0863, 451.1020, 543.0897, 559.1215, 577.1325, 587.1165, 677.1337, 695.1378, 713.1484, 739.1639, 847.1877	C-type proanthocyanidin	Flavanol
L10	447.0927	3.53	281, 369	$C_{21}H_{20}O_{11}$	−1.42	151.0031, 178.9980, 227.036, 255.0293, 301.0346	Quercetin *O*-rhamnoside	Flavonol
L11	391.1606	3.58	281, 369	$C_{17}H_{28}O_{10}$	−0.99	99.0451, 125.0239, 247.119, 289.1285, 329.1606, 345.1543, 365.2539	Unidentified	Unidentified
L12	577.1340	3.58	281	$C_{30}H_{26}O_{12}$	−1.93	245.0808, 273.0384, 287.0553, 289.0711, 299.0552, 381.0951, 407.0758, 425.0863, 433.0942, 451.102	B-type proanthocyanidin	Flavanol
L13	609.1451	3.58	281, 369	$C_{27}H_{30}O_{16}$	−1.58	301.0345	Rutin*	Flavonol
L14	431.0978	3.59	281, 326	$C_{21}H_{20}O_{10}$	−1.23	283.0595, 311.0554, 341.0662, 371.1157, 413.085	Apigenin *C*-glucoside	Flavone
L15	463.0876	3.61	281, 369	$C_{21}H_{20}O_{12}$	−1.4	151.0034, 178.9982, 255.064, 271.0232, 273.0387, 287.0545, 299.0192, 300.0268, 300.0713, 301.0345, 313.0346, 343.0451, 445.0747	Quercetin 3-*O*-glucoside*	Flavonol
L16	379.1032	3.62	282, 326, 443	$C_{18}H_{20}O_9$	0.7	137.0245, 155.035, 163.0401, 173.0455, 215.0559, 233.0665, 319.0819, 337.0924	Unidentified	Unidentified

(Continues)

TABLE 2 (Continued)

Peak no.	[M-H]⁻ (*m/z*)	Rt (min)	UV (nm)	Molecular formula	Error (ppm)	MS/MS product ions (*m/z*)	Identification	Metabolite class
L17	447.0929	3.67	284, 369	$C_{21}H_{20}O_{11}$	−0.87	151.0033, 178.9982, 227.035, 255.0296, 257.0439, 269.0453, 285.0394, 299.0557, 327.0503, 357.0609	Kaempferol *O*-glucoside	Flavonol
L18	445.0771	3.69	284, 326	$C_{21}H_{18}O_{11}$	−1.10	129.0193, 157.0149, 175.025, 269.0456, 311.0565, 341.0669, 427.0674	Apigenin *O*-glucuronide	Flavone
L19	461.0718	3.71	284, 326	$C_{21}H_{18}O_{12}$	−1.67	268.0354, 285.0402, 327.0492, 357.0602, 417.082, 443.0631	Kaempferol *O*-glucuronide	Flavonol
L20	717.1452	3.72	284, 326	$C_{36}H_{30}O_{16}$	−1.26	325.0351, 385.0718, 403.0819, 429.0612, 493.0923, 537.0824, 555.0931, 565.1344, 591.1137, 623.1032, 673.1552	Fukugiside	Biflavone
L21	641.2228	3.90	219, 280, 322, 369	$C_{33}H_{38}O_{13}$	−1.85	315.1224, 451.1971, 477.1773, 553.2464, 597.2336, 623.2125	Unidentified	Unidentified
L22	327.0869	4.35	222, 304, 366	$C_{18}H_{16}O_6$	−1.43	258.0166, 271.0243, 272.0314, 283.0242, 299.0917, 312.0629	Tetrahydroxy prenyl xanthone	Prenylated xanthone
L23	379.1552	4.51	289, 366	$C_{23}H_{24}O_5$	+0.14	145.0281, 269.08, 282.0878, 310.0817, 311.1644, 351.1567	Trihydroxy diprenyl xanthone	Prenylated xanthone
L24	533.2911	4.91	224, 289, 348	$C_{33}H_{42}O_6$	+0.40	309.1120, 379.1535, 393.1700, 464.2192	Polyprenylated benzophenone derivative	Polyprenylated benzophenone
L25	517.2953	5.04	224, 289, 345	$C_{33}H_{42}O_5$	−1.27	250.1209, 287.1287, 363.1597, 433.2015, 448.2251	Polyprenylated benzophenone derivative	Polyprenylated benzophenone
L26	407.1866	5.12	224, 366	$C_{25}H_{28}O_5$	+0.38	161.0235, 329.1386, 389.1738	Hydroxy-dimethoxy diphenyl xanthone	Prenylated xanthone
L27	365.1756	5.19	225, 297, 366	$C_{23}H_{26}O_4$	−0.56	145.0297, 219.1389, 253.0506, 255.1025, 267.0662, 287.1287, 321.1857	Clusiaphenone B	Polyprenylated benzophenone
L28	379.2643	5.23	225, 297, 366	$C_{26}H_{36}O_2$	−0.01	175.0764, 256.1463, 324.2087, 364.2399	Tocotrienol type	Tocotrienol
L29	441.2643	5.23	225, 297, 366	$C_{27}H_{38}O_5$	−0.76	151.0401, 379.2632, 397.2737, 423.2532	5-Hydroxy tocotrienoloic acid (N13)	Tocotrienol
L30	471.2745	5.37	225, 312, 345	$C_{28}H_{40}O_6$	−1.50	290.1521, 395.2592, 439.248, 453.2631	Unidentified	Unidentified
L31	363.1600	5.40	225, 366	$C_{23}H_{24}O_4$	−0.41	145.0295, 241.1224, 285.1130, 294.0894, 319.1700, 345.1494	Polyprenylated benzophenone derivative	Polyprenylated benzophenone
L32	425.2692	5.48	225, 366	$C_{27}H_{38}O_4$	−1.26	135.0452, 162.0688, 175.0762, 190.1, 203.1806, 245.1545, 258.1623, 289.2172, 363.2667, 379.2641, 381.2789, 407.2587	Tocotrienoloic acid	Tocotrienol
L33	431.2224	5.59	225, 289, 366	$C_{28}H_{32}O_4$	−0.93	271.1338, 327.1962, 363.1597, 417.2066	Machuone	Polyprenylated benzophenone
L34	433.2380	5.68	nd	$C_{28}H_{34}O_4$	−0.98	228.0427, 253.0506 296.105, 321.1130, 336.1727, 364.1676	Grandone	Polyprenylated benzophenone

TABLE 2 (Continued)

Peak no.	$[M-H]^-$ (m/z)	Rt (min)	UV (nm)	Molecular formula	Error (ppm)	MS/MS product ions (m/z)	Identification	Metabolite class
L35	499.2856	5.91	224, 289, 366	$C_{33}H_{40}O_4$	+0.52	285.1848, 325.1802, 349.1439, 430.2138, 463.2455	Polyprenylated benzophenone derivative	Polyprenylated benzophenone
L36	501.3006	6.03	225, 289, 348	$C_{33}H_{42}O_4$	−0.93	234.1257, 271.1334, 280.1105, 295.0964 327.1959, 363.1592 417.2058 432.2290, 457.3097	Nemorosone (N12)	Polyprenylated benzophenone
L37	501.3006	6.53	225, 280, 360	$C_{33}H_{42}O_4$	−0.81	441.2706, 457.3100	Polyprenylated benzophenone derivative	Polyprenylated benzophenone
L38	501.3009	6.68	225, 286, 362	$C_{33}H_{42}O_4$	−0.26	432.2300, 457.3109	Polyprenylated benzophenone derivative	Polyprenylated benzophenone
L39	411.2902	6.98	225, 289, 348	$C_{27}H_{40}O_3$	−0.67	151.0402, 206.0948, 274.1573, 342.2199, 393.2795, 396.2666	5-Hydroxy-8-methyltocotrienol (N14)	Tocotrienol
L40	569.3631	7.03	225, 289, 348	$C_{38}H_{50}O_4$	−0.94	271.2067, 355.2634, 377.1753, 432.2303, 525.3738	Polyprenylated benzophenone derivative	Polyprenylated benzophenone

*Confirmed with authentic standards. Product ions in bold represent base peaks in MS/MS spectra.

correlations shown in Figure S4 and a UPLC-MS peak that can be readily observed eluting at an earlier time point of 0.37 min with $[M-H]^-$ at *m/z* 191.0196 (peak **L1**) (Figure 2) considering its polarity.

In the hydroxy methine region (δ_H 5.5–3.4 ppm) of the NMR dataset, most signals are ascribed to protons of sugar units. Major sugars identified in all extracts belong to sucrose (**N4**), α-glucose (**N5**), β-glucose (**N6**), and fructose (**N7**), identified based on their anomeric protons at δ_H 5.38, 5.10, 4.46, and 4.01 ppm, respectively (Table 3).

Among the detected phenolic acids, and likely to contribute to plants' taste and further health effects, *p*-coumaroylquinic acid (**L4**, **N8**) was a major constituent detected in fruits and seeds of *C. minor*. Its identification was based on both UPLC-MS and NMR analyses, as not all NMR signals could be assigned in the crude extract spectra due to signal overlap and highlighting the benefit of data acquisition from both platforms (Table 3). Visualisation of the UPLC-MS trace of seed extract indicated that a major peak eluting at 1.46 min with a $[M-H]^-$ at *m/z* 337.0926 (Table 2) was a *p*-coumaroyl derivative. On the other hand, in leaves chlorogenic acid (**L6**, **N9**) was the dominant phenolic acid detected by using both UPLC-MS and NMR. This was also confirmed by comparison with authentic standard.

The largest subclass of flavonoids found in *C. minor* belonged to flavanols. Catechin (**L5**, **N10**) and epicatechin (**L8**, **N11**) were detected by both UPLC-MS and NMR in all samples, though at different levels. Well-resolved aromatic ^{1}H-NMR signals were detected for both catechin (**N10**) and epicatechin (**N11**) (Table 3). NMR chemical shifts are in accordance with those previously published for catechin and epicatechin.[31]

Compared with flavanol monomer detected using NMR and LC/MS, flavanol dimers were identified by UPLC-MS. For example, proanthocyanidin B2 (**L6**) was confirmed with an authentic reference sample, while peaks **L3** and **L12** were assigned to other proanthocyanidin B variants, based on their $[M-H]^-$ at *m/z* 577.1342 and characteristic fragmentation patterns. In addition, a C type proanthocyanidin was tentatively identified in peak **L9** (Table 2), not observed in NMR due to its low abundance.

Other flavonoid subclasses detected in *C. minor* were flavonols and flavones, though at lower levels compared with flavanols. They are readily detected using LC/MS, mostly found as glycosides of quercetin, kaempferol and apigenin aglycones, that is, rather ubiquitous flavonoids *in planta*. Confirmation of the aglycones was based on MS/MS signals of the quercetin residue at *m/z* 301 ($C_{15}H_9O_7^-$) in quercetin *O*-rhamnoside (**L10**), rutin (**L13**), and quercetin 3-*O*-glucoside (**L15**). Two kaempferol derivatives were likewise assigned in peaks **L17** and **L19**. Apigenin *C*-glucoside and apigenin *O*-glucuronide were tentatively identified in peaks **L14** and **L18**, respectively (Table 2). The biflavone Fukugiside, previously isolated from multiple *Garcinia* species,[32,33] was assigned in **L20**. This biflavone was found exclusively in UPLC-MS traces of fruits and seeds and suggests that these organs represent a potential source of this strong antioxidant.[34]

While flavonoids are ubiquitous *in planta*, xanthones are found in a limited number of families only, including Clusiaceae.[35] Three xanthones were detected in *C. minor* extracts, with annotations limited to their level of hydroxylation and prenylation, based on their MS/MS

TABLE 3 ^{1}H- and ^{13}C-NMR data and key ^{1}H-^{13}C HMBC correlations of metabolites identified in *Clusia minor* L. methanol extract (CD_3OD, 600 MHz for ^{1}H and 150 MHz for ^{13}C).

No.	Metabolite	Position	δ_H[a] (J in Hz)	δ_C[b], type	HMBC (H to C)
N1	Fatty acids	1	-	174.7, COOH	
		2, CH_2	2.325 t (7.8)	35.0	1, 3, 4
		3, CH_2	1.617 s	25.9	2, 4
		4, CH_2	1.31	30.1	
		ω, CH_3	0.895 t (7.3)	14.5	ω-1, ω-2
		ω-2, CH_2	1.28	32.8	
		ω-1, CH_2	1.31	23.8	
N2	Linoleic acid	11, CH_2	2.775 t (6.7)	26.4	9, 10, 12, 13
		9/10/12/13, CH	5.336, 5.341 m	129.1, 130.9	11
		18, CH_3	0.904 t (6.7)	14.5	
N3 L1	Citric acid	1, COOH	-	177.6	
		2, C	-	74.3	
		3a, CH_2	2.904 d (15.5)	44.2	1, 2, 4
		3b, CH_2	2.776 d (15.5)		1, 2
		4, COOH	-	173.9	
N4	α-Sucrose	1, CH	5.385 d (3.8)	93.6	2
		2, CH	3.428 dd (9.8, 3.8)	73.2	1
N5	α-Glucose	1, CH	5.100 d (3.8)	94.0	
N6	β-Glucose	1, CH	4.465 d (7.8)	98.2	
N7	Fructose	2, CH	4.092 d (8.2)	79.3	4
		4, CH	4.014 d (7.5)	75.6	2
N8 L4	*p*-Coumaroylquinic acid	1′	-	127.3	-
		2′/6′, CH	7.45 d (8.6)	131.0	4′, 7′
		4′, C	-	161.1	-
		3′/5′, CH	6.80 d (8.6)	116.9	1′
		7′, CH	7.65 d (16.0)	146.3	2′/6′, 9′
		8′, CH	6.37 d, (15.9)	116.0	1′
		9′, COOH	-	168.8	-
N9 L6	Chlorogenic acid	8′, CH	6.278 d (15.9)	114.9	3′
		7′, CH	7.576 d (15.9)	147.1	5′
		2′, CH	7.052 d (2.2)	115.2	8′, 3′, 6′
		5′, CH	6.958 dd (2.2, 8.0)	122.9	5′, 6′, 7′
		6′, CH	6.780 d (8.0)	116.5	5′
		3, CH	4.174 m	71.3	5
		4, CH	3.730 dd (2.7, 10.0)	73.4	4, 6
		5, CH	5.339 m	72.0	5
N10 L5	Catechin	2, CH	4.561 d (7.5)	82.8	3, 4, 1′, 2′, 6′
		3, CH	3.97 m	68.8	
		4, CH_2	2.85 dd (16.0, 5.0) 2.49 dd (16.0, 8.0)	28.6	
		6, CH	5.928 d (2.3)	96.1	10
		8, CH	5.853 d (2.3)	95.5	10
		10, C	-	100.6	
		1′, C	-	132.2	
		2′, CH	6.835 d (2.0)	115.2	2, 4′, 6′
		4′, C	-	146.1	

TABLE 3 (Continued)

No.	Metabolite	Position	δ_H[a] (J in Hz)	δ_C[b], type	HMBC (H to C)
		5′, CH	6.76 m	116	
		6′, CH	6.716 dd (8.2, 2.0)	119.9	2, 2′, 4′
N11 L8	Epicatechin	2, CH	4.81 (br. s)	79.9	1′, 2′, 6′
		6, CH	5.909 d (2.3)	95.6	8, 10
		8, CH	5.943 d (2.3)	95.3	6, 10
		10, C	-	99.9	
		1′, C	-	132.2	
		2′, CH	6.835 d (2.0)	115.2	
		6′, CH	6.789 dd (8.3 2.0)	119.9	2, 1′, 2′
N12 L36	Nemorosone	1, C	-	78.3	-
		3, C	-	120.6	-
		5, C	-	62.1	-
		6, CH_2	1.410 t (12.7)	42.3	7, 27
			2.008 dd (13.4, 4.0)		7, 28, 29
		7, CH	1.744 m	44.6	
		8, C	-	48.6	-
		9, C	-	210.2	-
		17, CH_2	3.092 qd (14.5, 7.2)	22.6	3, 18, 19, 20, 21
		10, CO	-	195.4	-
		11, C	-	138.5	-
		12/16, CH	7.581 dd (8.0, 1.0)	129.6	14, 10
		13/15, CH	7.244 t (8.0)	128.7	12/16, 14, 11
		14, CH	7.419 tt (8.0, 1.0)	133.0	12/16, 11
		18, CH	5.105 tt (7.2, 1.4)	122.9	17, 20, 21
		19, C	-	132.9	-
		20/30, CH_3	1.642 s	26.0	19, 24
		21, CH_3	1.587 s	18.0	20
		22, CH_2	2.487 qd (14.3, 7.0)	30.5	5, 6, 9, 23, 24
		23, CH	5.012 m	121.2	5, 22, 25, 26
		24, C	-	134.8	-
		26, CH_3	1.659 s	18.3	
		27, CH_2	1.729 m	28.3	
			2.143 dd (12.1, 6.0)		7, 28, 29
		28, CH	5.012 m	124.2	7, 27, 30, 31
		29, C	-	134.0	-
		25, CH_3	1.681 s	26.3	
		31, CH_3	1.642 s	18.1	
		32, CH_3	1.342 s	24.4	1, 7, 8, 33
		33, CH_3	1.096 s	16.3	1, 7, 8, 32
N13 L29	5-Hydroxy tocotrienoloic acid	2, C	-	75.6	
		3, CH_2	1.71–1.77 m	32.2	2, 10
		4, CH_2	2.638 td (7.0, 2.2)	18.4	2, 5, 6, 9
		5, C		146.3	
		6, C		141.8	
		7, CH	6.433 s	116.2	5, 6, 8, 9, 10, 11
		8, C	-	116.9	

(Continues)

TABLE 3 (Continued)

No.	Metabolite	Position	δ_H[a] (J in Hz)	δ_C[b], type	HMBC (H to C)
		9, C		137.7	
		10, C		110.7	
		11, CH_3	2.008 s	15.7	5, 6, 7, 8, 9, 10
		1′, CH_2	1.50–1.56 m	40.7	2, 17, 2′, 3′, 4′
		2′, CH_2	2.09 m	23.2	2, 1′, 3′, 4′
		3′/7′, CH	5.127 m	126.2	2′, 5′, 6′, 9′, 16′
		4′, C	-	135.7	
		5′, CH_2	1.96 m	40.7	3′/7′, 4′, 6′
		6′, CH_2	2.08 m	27.5	3′/7′, 4′, 5′
		8′, C	-	134.9	
		9′, CH_2	2.07 m	39.4	7′, 8′, 10′,11′, 15′
		10′, CH_2	2.273 q (7.4)	28.3	8′, 9′, 13′, 14′
		11′, CH	6.752 td (7.4, 1.5)	142.9	9′, 10′, 12′, 13′, 14′
		12′, C	-	129.5	
		13′, CH_3	1.787 s	12.7	11′, 12′, 13′
		14′, COOH	-	172.2	
		15′/16′, CH_3	1.585 s	16.1	3′/7′, 4′
		17, CH_3	1.234 s	24.3	2, 3, 4
N14 L38	5-Hydroxy-8-methyltocotrienol	2, C	-	75.6	
		3, CH_2	1.71–1.78 m	32.2	2, 4, 10, 1′, 17′
		4, CH_2	2.64 m	18.3	2, 10
		5, C	-	146.2	
		6, C	-	141.7	
		7, CH	6.435 s	116.9	5, 6, 9, 10, 11
		9, C	-	137.7	
		10, C	-	110.7	
		11, CH_3	2.008 s	15.7	5, 6
		1′, CH_2	1.48–1.53 m	40.2	2′, 3′, 17′
		2′, CH_2	2.09–2.13 m	23.2	2, 1′, 3′, 4′
		3′, CH	5.130 m	125.8	2′, 5′, 16′
		4′/8′, C	-	135.8	-
		5′, CH_2	1.95–1.98 m	40.7	4′, 7′
		6′, CH_2	2.03–2.09 m	27.4	4′/8′, 5′, 7′
		7′, CH	5.075 m	125.6	9′, 15′
		9′, CH_2	1.92–1.94 m	40.7	8′, 11′
		10′, CH_2	2.03–2.09 m	27.7	8′, 9′, 11′, 12′
		11′, CH	5.075 m	125.2	9′, 10′, 14′
		12′, C	-	131.9	-
		13′, CH_3	1.582 s	17.8	12′
		14′, CH_3	1.654 s	25.9	11′, 12′, 13′
		15′, CH_3	1.563 s	16.1	
		16′, CH_3	1.570 s	15.8	
		17′, CH_3	1.234 s	24.4	2, 3, 1′

Abbreviations: d, doublet; dd, doublet of doublet; HMBC, heteronuclear multiple-bond correlation; HSQC, heteronuclear single-quantum coherence, m, multiplet; NMR, nuclear magnetic resonance; qd, quartet of doublets; s, singlet; t, triplet; td, triplet of doublets; tt, triplet of triplets.

[a]^{1}H chemical shifts with only two decimal places are chemical shifts of HSQC correlation peaks or signal overlapping.

[b]Chemical shifts of HSQC or HMBC correlation peaks.

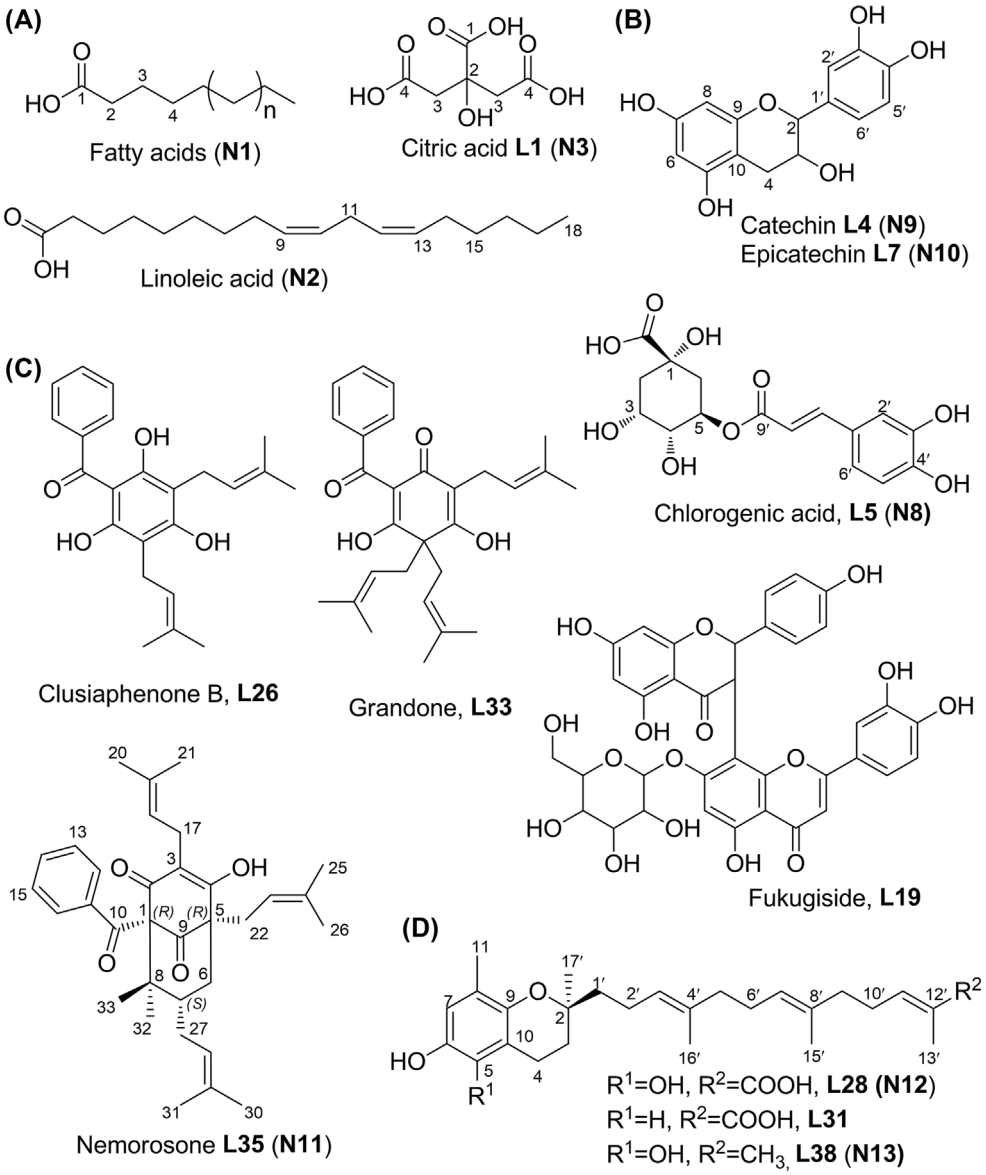

FIGURE 3 Chemical structures of metabolites identified in *Clusia minor* L. methanol extracts. Organic acids (A), phenolics and flavonoids (B), polyprenylated benzophenone (C), and tocotrienols (D). Note the carbon numbering system for the compounds is used throughout the manuscript for NMR assignment and thus is based on analogy rather than International Union of Pure and Applied Chemistry (IUPAC) rules. L and N prior to compound numbers denote the identification techniques UPLC-MS and NMR, respectively.

fragmentation pattern. **L22** was annotated as tetrahydroxy (mono)prenyl xanthone, while **L23** as trihydroxy diprenyl xanthone. Compounds with these structures have been isolated from several *Garcinia* species (Clusiaceae) and are believed to contribute to their antidiabetic activity and cytotoxic effect against cancer cell lines.[36,37] **L26** was assigned to hydroxy-dimethoxy diphenyl xanthone and can be annotated as 3,5-Di-*O*-dimethyl-8-deoxy-gartanin, a compound previously reported from the floral resin of *Clusia nemorosa*.[38]

Another class of secondary metabolites widely distributed and typical in the Clusiaceae are polyprenylated benzophenones.[17] A total of 11 UPLC-MS peaks showed molecular formulas and MS/MS fragmentation pattern characteristic of that class. Fragments include mostly sequential losses of 69 amu (–C_5H_9, prenyl groups) and 18 amu (-H_2O, hydroxyl groups) (Table 3) and aided in their structural elucidation.[39,40] Clusiaphenone B (**L27**), machuone (**L33**), and grandone (**L34**) were major forms and have been previously detected in *Clusia sandiensis* fruits.[41,42] **L27** was detected in all *C. minor* organs, but its level was much higher in flowers. **L33** seems to be present only in flowers, whereas **L34** was found in all organs but at much lower levels in the leaves (Figure 1). Profiling results suggest that among *C. minor* organs, flowers are the most enriched ones in polyprenylated benzophenones, probably based on the pollination biology, rewarding bees with such compounds. Considering our interest in that class and to fully elucidate its major compounds detected in the flowers (Figure 2), (**L36**, **N12**) was isolated and analysed using UPLC-MS and NMR for full structure characterisation. Data were compared with the literature,[43] and the constituent was confirmed as nemorosone (**L36**, **N12**). Complete ^{1}H and ^{13}C-NMR assignments are presented in Table 3, and extensive NMR spectra are presented in Figure S5–S8. Nemorosone was previously found as the major component in the floral resins of Clusias like *Clusia rosea*, *Clusia grandiflora*, *Clusia insignis*, and *C. nemorosa*.[42] Although other Clusiaceae genera are also reported for yielding bicyclic polyprenylated acylphloroglucinols (BPAPs), nemorosone has only been described in the name-giving

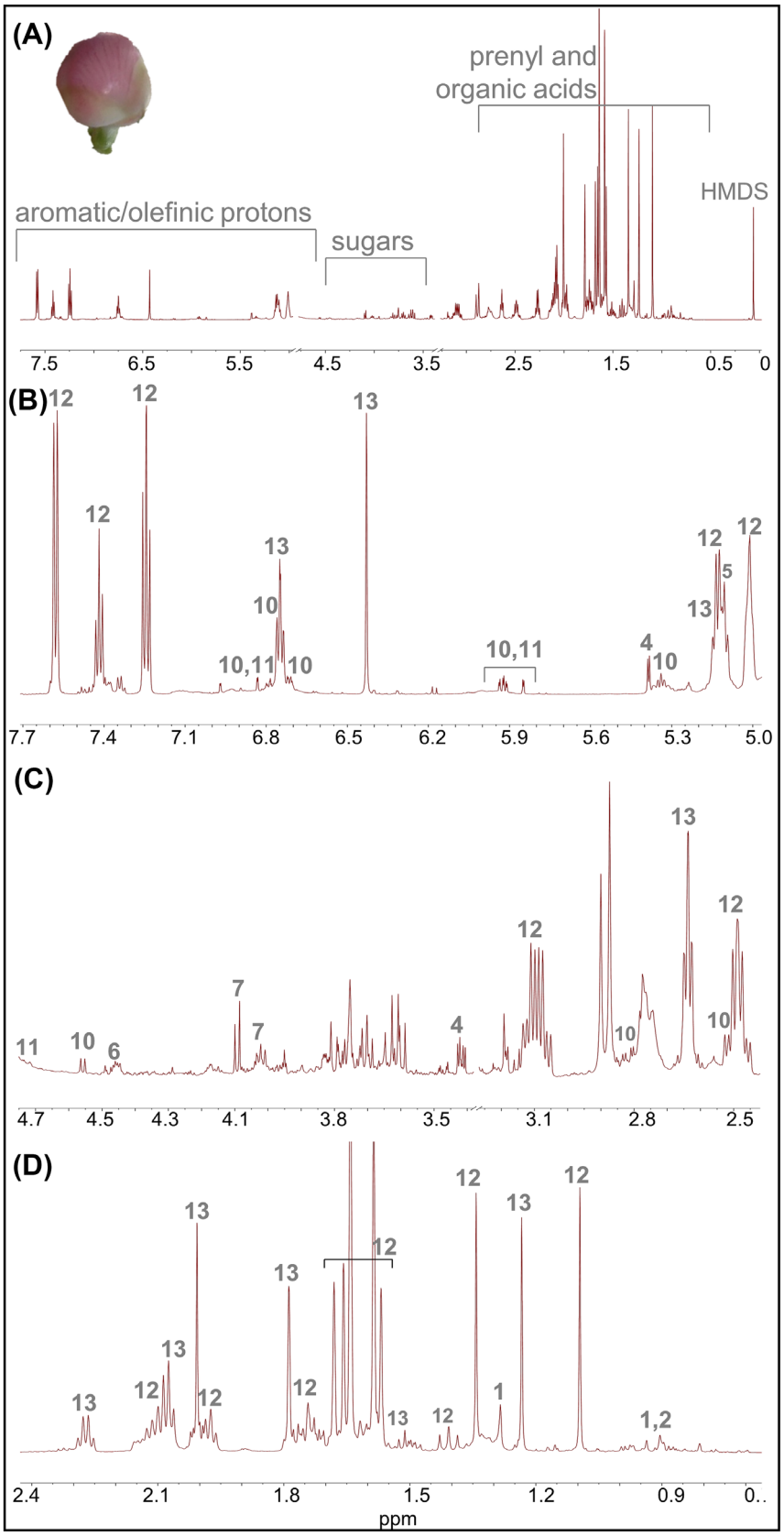

FIGURE 4 1H NMR spectrum of the fully mature bud flower (FL6) of *Clusia minor* L. in CD3OD showing characteristic signals for metabolites in the most relevant shift range (δ 0.0–7.5 ppm) (A). Expanded spectral region from 5.0–7.7 (B), 2.5–4.7 (C), and 0.7–2.4 ppm (D) with assigned peaks: N1 (fatty acids), N2 (linoleic acid), N4 (α-sucrose), N5 (α-glucose), N6 (β-glucose), N7 (fructose), N9 (chlorogenic acid), N10 (catechin), N11 (epicatechin) N12 (nemorosone), and N13 (5-hydroxy tocotrienoloic acid). Signal numbers correspond to those listed in Table 3 for metabolite identification using NMR spectroscopy. [Colour figure can be viewed at wileyonlinelibrary.com]

Clusia genus species thus far, with *C. minor* now added as another potential source of that phytochemical. A comprehensive review focusing on nemorosone effects recently has been published[44] considering its potential pharmacological effects including cytotoxicity against malignant cells and antiparasitic and antimicrobial properties.

Tocotrienols are commonly concentrated during seed development.[45–47] Their derivatives represent another type of prenylated compounds found in *Clusia*.[7] Prenyltransferases involved in the production of these phytochemicals have yet to be cloned. Using UPLC-MS, four peaks were annotated as tocotrienol derivatives including **L28**, **L29**, **L32**, and **L39**. The structure of **L28** could not be confirmed, whereas **L32** was annotated as tocotrienoloic acid (garcinoic acid), a compound previously isolated from various *Clusia* species: *Clusia obdeltifolia*,[48] *Clusia burle-marxii*,[49] *C. pernambucensis*,[16] and *Clusia criuva*.[5] Garcinoic acid shows many bioactive properties including antioxidant, antiproliferative, anti-inflammatory,[50,51] and hypoglycemic activities.[52]

A derivative of garcinoic acid was identified to cause peak **L29** with $[M-H]^-$ at *m/z* 441.2643 ($C_{27}H_{38}O_5$) with one oxygen atom more than garcinoic acid. **L29** was the second most abundant compound in *C. minor* flowers and was isolated using HPLC for further structure elucidation. Its MS/MS spectrum showed a major fragment at *m/z* 397.2737 $[M-CO_2-H]^-$ and other product ions corresponding to the loss of H_2O (*m/z* at 423.2532), followed by subsequent loss of CO_2 (*m/z* at 379.2632) (Table 2). Extensive NMR experiments were carried out (Figure S9–S12), and **L29** (**N13**) was identified as 5-hydroxy tocotrienoloic acid (Table 3), based on comparison with the reported data for garcinoic acid.[53] The garcinoic acid NMR spectrum presents two aromatic protons (H-5 and H-7) appearing as two doublets at δ_H 6.37 (J = 2.7 Hz) and 6.47 ppm (J = 2.7 Hz), respectively.[53] While 5-hydroxy tocotrienoloic acid identified herein exhibited only one singlet at δ_H 6.43 ppm assigned to H-7 (δ_C 116.2 ppm). The NMR signal for H-11′ appeared at δ_H 6.75 ppm (td, J = 7.4, 1.5 Hz), displaying HMBC correlations with δ_C 12.7 (CH_3–13′), 28.3 (CH-10′), 129.5 (C-12′), and 172.2 (C-14′), consistent with a prenyl side chain oxidised at the terminal position (Figure S13). In summary, **L29** structure differed from garcinoic acid by an extra OH group at position C-4. A hydroxylated garcinoic acid has been described in the gum resin of *Garcinia kola*[54]; however, the authors presented only UPLC-MS data for this compound. This is the first report of the NMR data of 5-hydroxy tocotrienoloic acid in literature (**L29**, **N13**).

Another tocotrienol derivative, (**L39**, **N14**), was detected in *C. minor* organs with highest levels in leaves and early flower stages. Its NMR signals presented a similar pattern to (**L29**, **N13**), but without the carboxylic acid moiety at the terminal position (C-14′). This is evident from the key cross peaks of δ_H at 1.65 ppm (H-14′) and δ_C at 17.8 (CH_3-13′), 125.2 (CH-11′), and 131.9 ppm (C-12′) in the HMBC spectrum (Figure S14). With a predicted molecular formula calculated obtained from UPLC-MS of $C_{27}H_{40}O_3$ (Table 2), this compound was identified as 5-hydroxy-8-methyltocotrienol. It has been isolated only recently from the roots and branches of *Allophylus cobbe* (L.) Raeusch.[55] The NMR signals for 5-hydroxy-8-methyltocotrienol (**L39**, **N14**) and other major leaf compounds can be better visualised in the leaf ^{1}H-NMR spectrum, as shown in Figure S15.

3.2 | Multivariate data analysis of UPLC-MS and ^{1}H- and ^{1}H-^{13}C-HMBC-NMR datasets

Metabolomics studies typically generate large datasets, and for assisting in identifying variations among the different developmental stages of *C. minor* organs in an untargeted manner, multivariate data analysis of spectral datasets was adopted. Chemometric tools are routinely applied to 1D-NMR spectra,[56] but less has been done with 2D-NMR fingerprints, introducing another set of chemical shifts from the carbon dimension. Such 2D-spectra like HMBC spectra could complicate the spectral processing. We have previously developed a novel (to our knowledge the first ever) approach in coupling HMBC datasets with PCA for hop resin classification,[30] which we extend herein for the ontogenic study in *Clusia*. Details for spectral processing are described in the same report.[30] Briefly, complex HMBC spectra were divided into small pixel areas (=2D bins) comprised of 0.04 ppm in the ^{1}H dimension and 0.92 ppm in the ^{13}C dimension and spectral intensities to generate a 2D-NMR matrix.

PCA was employed to explore the relative variability within different organs. The PC1 plotted against PC2 scores derived from UPLC-MS (Figure 5A), 1D ^{1}H-NMR (Figure 5B) and 2D ^{1}H-^{13}C-HMBC-NMR (Figure 5C) datasets revealed four distinct major clusters, each one corresponding to a plant organ (viz. leaves, flowers, fruits, and seeds). Replicates (biological and technical) were found to cluster together confirming the high reproducibility of the extraction and detection method.

The first two components of the UPLC-MS dataset explained 77% of the variance (Figure 5A), and its loadings plot (Figure 5D) indicated that the polyprenylated benzophenones nemorosone and grandone contributed most to the segregation of the flower samples. In contrast, leaf samples were rich in citric acid and 5-hydroxy-8-methyltocotrienol, while fruits were elevated in 5-hydroxy tocotrienoloic acid and a not yet identified polyprenylated benzophenone derivative (**L37**).

Similar PCA results were observed in 1D- and 2D-NMR-derived score plots, although with HMBC-NMR accounting for a smaller total variance of 24% along PC1 and PC2 compared with 62% in the case of ^{1}H-NMR (Figure 5B & 5C). This is likely attributed to the low detection level of HMBC compared with ^{1}H-NMR. As expected, seeds as storage organ appeared the most distant from other organs being enriched in fatty acids (Figure 5E & 5F) and tocotrienol derivatives. Loading plots from both datasets were examined to highlight NMR resonances that contribute significantly to organ differentiation. The variables are δ_H buckets in the case of 1D- and cross peak pixels in the case of 2D-NMR HMBC datasets. Similar results were revealed from both loading plots. Nemorosone (**N12**) was found enriched in flowers, while citric acid has its highest abundance in leaves. Expectedly, this suggests that flowers present the best source of

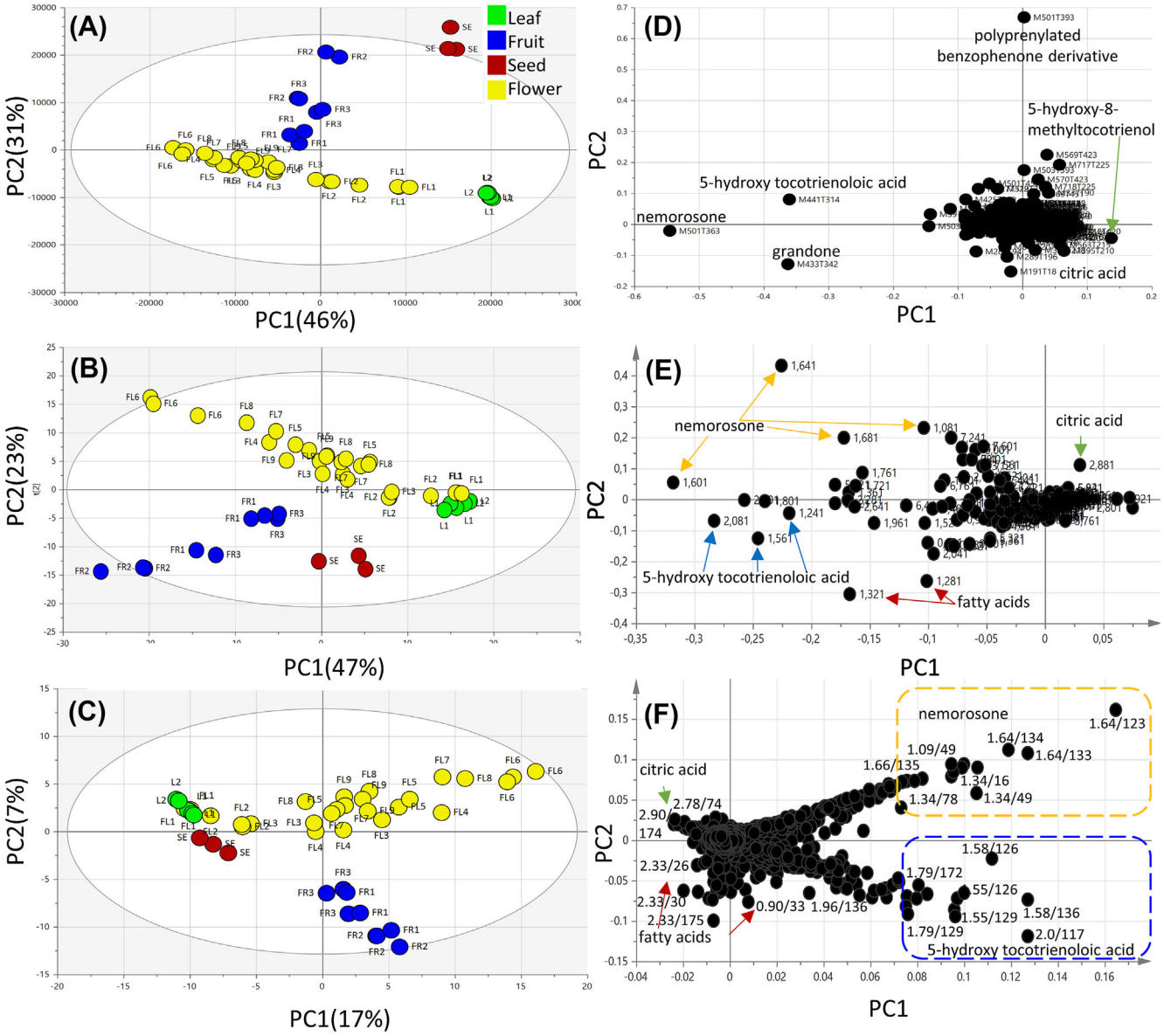

FIGURE 5 Principal component analysis (PCA) score plots derived from UPLC-MS (A), 1H-NMR (B), and 1H-13C HMBC-NMR (C) datasets of different developmental stages of *Clusia minor* L. organs. Respective loading plots with contributing assignments to the mass peaks (D), proton chemical shifts (E), and cross peak pixels (F). Sample colours: green (leaves—L), yellow (flowers—FL), blue (fruits—FR), and red (seeds—SE). Sample code details are explained in Table 1. [Colour figure can be viewed at wileyonlinelibrary.com]

polyprenylated benzophenones, the resinous substance collected by pollinating bees, in *C. minor*. This also is in agreement with other taxa such as hypericum.[1,25] The clustering of fruit specimens was mostly attributed to its richness in 5-hydroxy tocotrienoloic acid (**N13**), so that organ can act as a rich source of that unusual tocotrienol derivative.

Like PCA, HCA represents another unsupervised data analysis tool that allows easier interpretation of the results in an intuitive graphical way. HCA of the UPLC-MS-derived dataset revealed a dendrogram, in which four clusters were designated, comprising each one of the organs [viz. seeds (SE), fruits (FR), leaves (L), and flowers (FL)] (Figure 6A). Compared with UPLC-MS, 1D- and 2D-NMR spectra-derived dendrograms (Figure 6B & 6C) showed clusters that combined leaf samples with green flower bud stages likely for the comparable metabolome composition especially from primary metabolites readily to be detected in NMR and not UPLC-MS.

3.3 | Metabolite quantification in organs

Quantitative NMR (qNMR) measurement represents a reliable and well-established method for determining the concentration of compounds in mixtures. It uses the proportional relation of an integrated signal area and the number of nuclei corresponding to its resonance.[57] Well-resolved peaks for most of the identified metabolites described in Table 3 via 1D and 2D-NMR allowed an unbiased absolute

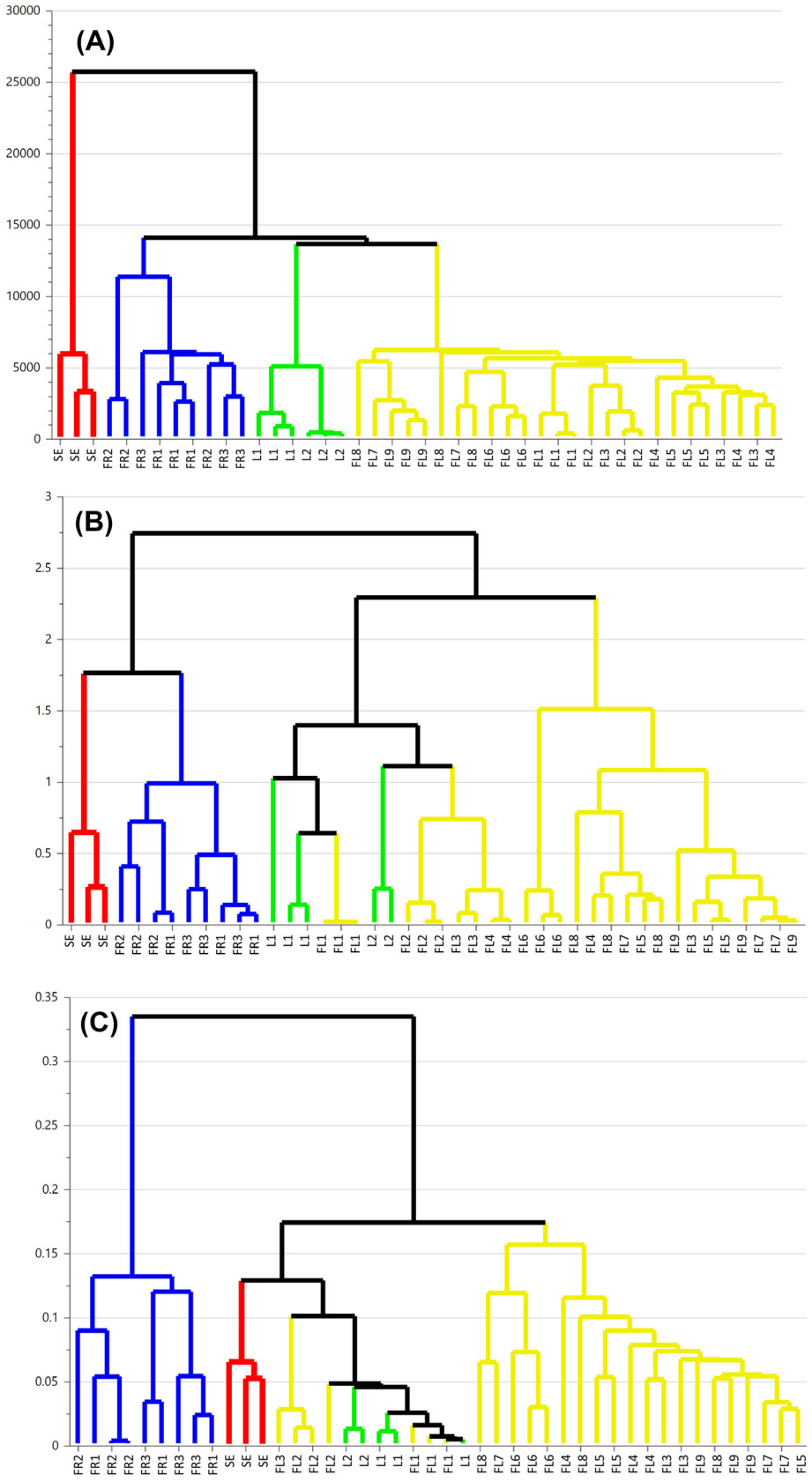

FIGURE 6 Hierarchical cluster analysis dendrograms from the UPLC-MS (A), 1H-NMR (B), and 1H-13C HMBC-NMR (C) datasets of modelling different developmental stages of *Clusia minor* L. organs. Colour lines: red (seeds—SE), blue (fruits—FR), green (leaves—L), and yellow (flowers—FL). Sample code details are explained in Table 1. [Colour figure can be viewed at wileyonlinelibrary.com]

quantification for their levels in all samples. Nevertheless, for the quantification to be optimal, full relaxation of the protons of target metabolite signals and the internal standard HMDS had to be achieved. For that, a rather large sum of relaxation delay and acquisition time of 25 s was employed for NMR acquisition, as the longest relaxation times were 4.5 s for the HMDS protons. For

quantifications, NMR signals unique to each metabolite and sufficiently separated from neighbouring signals were selected. Using qNMR, the concentration of some of these primary and secondary metabolites were calculated and are presented in Table 4, expressed as μg mg^{-1} fresh weight (μg mg^{-1} f.w.).

Plants concentrate allocation of resources according to their needs at certain stages. Growth, defence, and attraction/repulsion are some of their priorities under normal developmental conditions.[58] In this context, results presented in Table 4 highlight the great metabolic variability among the different organs of *C. minor*.

Seeds as energy storage organs encompassed the highest levels of sugars, that is sucrose, fructose (17.97 and 6.90 μg mg^{-1} f.w., respectively), and fatty acids such as linoleic acid (9.85 μg mg^{-1} f.w.). In fruits and seeds, secondary metabolites may act in the context of seed dispersal and fruit defence, by being associated with rewards for dispersers or by deterring predators and pathogens.[59]

Citric acid was only detected by ^{1}H-NMR in the leaves, with highest level found in mature leaves (**L2**) at ca. 136 μg mg^{-1} f.w. *C. minor* is a facultative water-conserving crassulacean acid metabolism (CAM) plant. This photosynthetic pathway is seen as a way to cope with drought[60] and to account for the high levels of citric acid to lessen photoinhibition. Then, under drought conditions, instead of increasing maximum photon utilisation, the plant will use the stored citric acid for carbon intake.[61] If it also adds to plant health needs to be examined.

Chlorogenic acid was also mostly observed in leaves, though with an opposite accumulation pattern to that of citric acid, being found at higher levels in the earlier leaf stage (**L1**) at 2 μg mg^{-1} f.w. It declines during flower development, until it is absent or reaches the detection limit in the fruits. A similar trend was observed during the flower development of *Lonicera japonica* Thunb.[62] Accumulation of chlorogenic acid in young tissues may be a defence mechanism against various stresses due to the antioxidant and antimicrobial potential of this phenolic compound,[63] especially in this critical stage in plant life.

Green bud flower stages (FL2, FL3, and FL4 with 3.58, 3.76, and 3.01 μg mg^{-1} f.w., respectively) showed the highest levels of catechins. Interestingly, epicatechin was found in larger amounts than catechin in most of the organs. In summary, the overall distribution of catechin and epicatechin in the different organs had the following abundance order: buds > flowers > leaves > fruits = seeds. It has been reported[64] that catechin and epicatechin are major flavonoids in rose petals and that their contents also reduced during flower development. Flavonoids can act as antioxidants and play a role in protecting the flower bud cells of reactive oxygen species caused by biotic or abiotic factors.[62]

Nemorosone as major polyprenylated benzophenone was not detected in leaves, and its concentration gradually increased during the budding stage until it reached its peak in the fully mature flower bud (FL6, ca. 60 μg mg^{-1} f.w.). This was followed by a steady decrease during flowering and a sudden decline when fruits are formed, with ca. 3 μg mg^{-1} f.w. left in the mature fruit (FR2) (Table 4). Polyprenylated benzophenones have their core structure derived from the shikimate and acetate-malonate pathways, with multiple isoprenyl substitutions at the phenyl(s). This type of compound has been previously described as the major secondary metabolite class in floral resins of several *Clusia* species, although they can be found in other organs, as revealed in our metabolomics approach. Polyprenylated benzophenones play an important ecological role acting as a reward to pollinating bees that collect these floral resins for nest construction. After slow, yet chemically not quite clear polymerisation, the resin provides a waterproof and probably antimicrobial protection, since the latter is an expected characteristic of benzophenones.[17,42] This is similar to the flower oil-based resins bees collect from the related Malpighiaceae but also other, unrelated genera for nest lining.[20–22,65] The prenyl group in the benzophenones increases their lipophilicity and likely the penetration into the bacterial cell to account for their antimicrobial actions. It also enhances oxidisability (and thus may initiate oxidative crosslinking in the bee nest lining).

A different metabolic function might be associated with the biosynthesis of tocotrienols. Only the leaves contained quantifiable levels of 5-hydroxy-8-methyltocotrienol (**N14**). In other organs, this compound was probably metabolised to 5-hydroxy tocotrienoloic acid (**N13**), by oxidation of one of the terminal methyls to a carboxylic acid group. The levels of **N13** constantly increase in the flowering tissue with most of it detected in the fully mature bud (FL6, ca. 43 - μg mg^{-1} f.w.), and eventually accumulating in the mature fruit FR2with 50 μg mg^{-1} f.w. among all samples (Table 4).

Tocotrienols are unsaturated forms of tocopherols (vitamin E isoforms) much less widespread in the plant kingdom than the latter. They both present a chromanol ring, albeit the side chain of tocotrienols contains three double bonds while the one in tocopherols is saturated. Although tocopherols are well known for their health benefits, studies indicate tocotrienols present a greater antioxidant potential than tocopherols.[66] Interestingly, tocotrienols are commonly enriched in seeds compared with tocopherols in other organs. We observed such enrichment earlier in seeds.[45–47] Seeds have to show a higher temperature and oxidation resistance and hence a greater membrane stability, which can be assigned to the more rigid trienols. Transgenic tocotrienol-accumulating plants also have shown greater phototolerance than their wild-type counterpart suggestive of an efficient in vivo antioxidant potential of these compounds via protection of membrane lipids from peroxidation.[67] Considering *C. minor* is a tropical plant that grows in sunny Amazonian and coastal Brazilian regions, the presence of 5-hydroxy-8-methyltocotrienol (**N14**) in its leaves suggests that this compound might exert photoprotectant, antioxidant, and membrane rigidification action.

Plants tend to allocate their resources to protect tissues or organ stages that are important towards their fitness. Production of secondary metabolites divert carbon reserves from tissue growth, and therefore the plant must follow a trade-off of fast growing, maintenance, reproduction, and defence through physiological adaptations for survival.[68,69] The metabolites identified in *C. minor* are a part of various biosynthetic pathways. The high levels of polyprenylated benzophenones and tocotrienol derivatives in flowers and fruits, respectively, suggest an important role in the attractiveness and protection of reproductive tissues in *C. minor* more favoured by the plant at this critical and culminative stage of its life.

TABLE 4 Metabolite levels expressed as μg mg^{-1} of fresh weight (f.w.) ± S. D ($n > 3$) in different organs of *Clusia minor* L. Results were obtained by ^{1}H-NMR analysis of extracts in CD_3OD versus standard.

	Samples					
Metabolites	**L1**	**L2**	**Fl1**	**Fl2**	**Fl3**	**Fl4**
Linoleic acid (N2)	Nq	Nq	2.75 ± 0.21^{a}	3.85 ± 0.32^{a}	3.58 ± 0.05^{a}	5.68 ± 0.93^{b}
Citric acid (N3)	83.15 ± 5.7^{c}	136.36 ± 7.2^{d}	nq	nq	nq	nq
Sucrose (N4)	8.33 ± 0.41^{b}	10.15 ± 0.93^{b}	6.24 ± 0.18^{a}	9.41 ± 0.99^{b}	8.58 ± 0.57^{b}	9.20 ± 0.39^{b}
Fructose (N7)	4.81 ± 0.50^{b}	5.16 ± 0.43^{b}	3.08 ± 0.14^{a}	5.07 ± 0.48^{b}	4.13 ± 0.40^{a,b}	4.57 ± 0.12^{b}
Chlorogenic acid (N8)	2.03 ± 0.09^{e}	1.72 ± 0.09^{d}	0.53 ± 0.02^{c}	0.59 ± 0.06^{c}	0.39 ± 0.05^{b}	0.32 ± 0.06^{b}
Catechin (N9)	1.33 ± 0.2^{a}	0.74 ± 0.1^{a}	2.69 ± 0.3^{b}	3.58 ± 0.5^{c}	3.76 ± 0.4^{c}	3.01 ± 0.4^{c}
Epicatechin (N10)	2.62 ± 0.4^{c}	1.34 ± 0.2^{a}	2.96 ± 0.1^{c}	3.96 ± 0.2^{d}	3.55 ± 0.3^{d}	2.77 ± 0.3^{c}
Nemorosone (N12)	nq	nq	1.04 ± 0.15^{a}	7.95 ± 0.74^{b}	21.46 ± 2.99^{c}	42.21 ± 3.02^{f}
5-Hydroxy tocotrienoloic acid (N13)	nq	nq	6.16 ± 0.65^{a}	18.79 ± 2.44^{b}	29.61 ± 2.43^{c}	33.31 ± 4.90^{c}
5-Hydroxy-8-methyltocotrienol (N14)	8.45 ± 0.53^{a}	6.19 ± 0.13^{a}	nq	nq	nq	nq

Note: Quantitation was carried out relative to the internal standard hexamethyldisiloxane (0.935 mM). Values are the mean ± SE of measurements made on biological and technical replicates. Sample codes refer to Table 1. a–h Different letters in a line (row) indicate significantly different values ($p < 0.05$; Tukey's test). nq = not quantified (Not detected or broad overlapping with neighbouring signals).

TABLE 4 (Continued)

	Samples								
Metabolites	**Fl5**	**Fl6**	**Fl7**	**Fl8**	**Fl9**	**Fr1**	**Fr2**	**Fr3**	**Se1**
Linoleic acid (N2)	2.99 ± 0.35^{a}	nq	nq	nq	nq	3.97 ± 0.48^{a,b}	4.75 ± 0.47^{a,b}	4.52 ± 1.00^{a,b}	9.85 ± 0.50^{c}
Citric acid (N3)	nq	nq	nq	nq	nq	nq	nq	nq	nq
Sucrose (N4)	7.85 ± 0.83^{a,b}	6.72 ± 0.52^{a,b}	8.52 ± 0.49^{b}	6.84 ± 0.71^{a,b}	10.35 ± 0.97^{b}	8.16 ± 0.78^{b}	8.66 ± 0.34^{b}	5.90 ± 0.59^{a}	17.97 ± 0.20^{d}
Fructose (N7)	4.02 ± 0.52^{a,b}	3.34 ± 0.28^{a}	4.14 ± 0.31^{a,b}	3.30 ± 0.53^{a,b}	5.37 ± 0.74^{b}	3.23 ± 0.23^{a}	3.32 ± 0.16^{a}	2.06 ± 0.12^{a}	6.90 ± 0.27^{c}
Chlorogenic acid (N8)	0.16 ± 0.01^{a}	0.13 ± 0.01^{a}	0.08 ± 0.01^{a}	0.08 ± 0.02^{a}	0.09 ± 0.02^{a}	nq	nq	nq	nq
Catechin (N9)	2.49 ± 0.4^{b}	2.38 ± 0.3^{b}	2.32 ± 0.4^{b}	1.52 ± 0.2^{a}	2.16 ± 0.2^{b}	0.63 ± 0.1^{a}	0.73 ± 0.1^{a}	0.53 ± 0.1^{a}	0.59 ± 0.2^{a}
Epicatechin (N10)	2.20 ± 0.3^{b}	1.85 ± 0.1^{b}	2.49 ± 0.6^{c}	1.49 ± 0.3^{a}	2.65 ± 0.2^{c}	1.05 ± 0.1^{a}	1.15 ± 0.1^{a}	1.07 ± 0.1^{a}	1.01 ± 0.1^{a}
Nemorosone (N12)	34.89 ± 2.90^{e}	60.14 ± 3.71^{h}	47.79 ± 3.40^{g}	44.45 ± 4.11^{f}	26.74 ± 0.86^{d}	8.35 ± 0.49^{b}	3.17 ± 1.09^{a,b}	3.99 ± 0.76^{a,b}	nq
5-Hydroxy tocotrienoloic acid (N13)	33.53 ± 1.23^{c}	42.95 ± 2.06^{d}	26.15 ± 2.32^{c}	21.37 ± 1.64^{b}	24.50 ± 2.10^{c}	43.38 ± 4.71^{d}	50.19 ± 3.09^{e}	38.75 ± 2.91^{c,d}	13.12 ± 2.41^{a,b}
5-Hydroxy-8-methyltocotrienol (N14)	nq	nq	nq	nq	nq	nq	nq	nq	nq

Note: Quantitation was carried out relative to the internal standard hexamethyldisiloxane (0.935 mM). Values are the mean ± SE of measurements made on biological and technical replicates. Sample codes refer to Table 1. a–h Different letters in a line (row) indicate significantly different values ($p < 0.05$; Tukey's test). nq = not quantified (Not detected or broad overlapping with neighbouring signals).

3.4 | Comparison of different technologies as biomarker screening tools

The results obtained by applying UPLC-MS and NMR-based metabolomics approaches to assess ontogenic changes in *C. minor* organs were presented for the first time in literature using such omics approaches. The 2D-NMR experiment performed herein is not yet routinely used in plant metabolomics studies,[1] and it has several advantages over 1D methods providing stronger structure elucidation power than that observed in the case of 1D-NMR and likewise MS. Also phase and baseline corrections, normalisation, and data analysis are simpler than for 2D-NMR data. However, longer acquisition times and more advanced instruments and software are needed for measurement in the case of 2D experiments. Yet, it should be noted that in our study both techniques (^{1}H and HMBC-NMR) required equal acquisition times of ca. 30 min per spectrum due to the long relaxation delay used in the 1D case for quantification purposes. Therefore, 1D analysis used in this study provided direct quantification of selected metabolites, while 2D analysis reduced spectral overlap and added molecular connectivity information that led to a clearer metabolite identification.

Yuk and colleagues[70] compared the potential of three different 1D- and 2D-NMR methods to discriminate earthworms exposed or not to a pesticide, and the best outcomes were found for the HSQC technique. In our study, both 1D- and 2D-NMR spectral data yielded accurate discriminations among the different organs. The results infer that leaves have the highest levels of citric acid and 5-hydroxy-8-methyltocotrienol and seeds are rich in sucrose and omega-6 fatty acids, flowers in polyprenylated benzophenone nemorosone, and fruits in 5-hydroxy tocotrienoloic acid, all fitting perfectly their ecological roles at their respective stages (Figure 7). Although HMBC is known to be less sensitive than ^{1}H-NMR, both techniques were able to provide accurate information on the different organs of *C. minor* using similar acquisition times and providing comparable statistical clustering results. Nevertheless, it is important to optimise the methods according to the type and concentration of compounds in the analysed samples. One of the drawbacks of ^{1}H-NMR fingerprinting is peak overlap, here resolved by 2D HMBC-NMR dispersing signals to two dimensions instead of one. Overall, 2D HMBC-NMR brings a third layer of complexity and contributes immensely to the compound identification confidence because it shows long-distance proton and carbon connectivity.

Multivariate data analyses of the datasets permitted the construction of chemometric models for data interpretation and marker identification. Comparing the three technologies, UPLC-MS was the one that explained most of the variance among the samples (77%) likely due to its higher sensitivity and better detection of secondary metabolites than primary ones, which are co-detected using NMR and which do not show many qualitative differences among organs. Comparison between NMR and UPLC-MS classification potential of liquorice drugs done earlier by us already revealed that UPLC-MS provides a stronger model attributed to its richness in MS signals for secondary metabolites with no detection of primary metabolites which are difficult to ionise using ESI source in UPLC-MS.[2] However, sample preparation can be more straight forward for NMR, and most of all, LCMS datasets are influenced by differential ionisation and ion suppression; therefore, peak areas cannot be directly related to compound concentrations in samples. ^{1}H-NMR data on the other hand allow absolute quantitation but are less sensitive than UPLC-MS, and therefore mostly major compounds are detected in the samples,[56] especially if no enrichment step (which can cause artefacts) was undertaken prior to data acquisition during sample preparation. The results presented here highlight the complementarity of the three experimental methods in explaining the phytochemical composition of the different organs of *C. minor*.

With regard to the NMR fingerprinting technology development, HMBC-NMR coupled to multivariate data analysis for *Clusia* organ classification as a test model was compared with that of 1D-NMR. For anonymous clustering of organ-specific constituents, 1D-NMR of direct extracts is sufficient and fast. However, for deeper insights and reliable annotation or especially new constituents, the long-range couplings in HMBC spectra (over two and three bonds) provide crucial information on the connectivity between carbons and hydrogens, resulting in a better assignment of metabolites in crude plant extracts.[30] HMBC cross peak patterns of metabolites are indeed a promising approach that in our opinion is underexplored for plant extract classification using multivariate data analysis and sound determination of discriminating constituents.

Finally, the samples were taken from a greenhouse-grown plant at IPB. We are aware that plants or other organisms grown under non-native conditions may show some deviation in their metabolite patterns (usually especially affecting flavonoid and terpenoid content)[71] However, the main process, especially in flower and fruit development, should be genetically fixed, and thus deviation from naturally grown specimen (which we could not access within reasonable time) should be minimal.

The current study represents the first comprehensive map of metabolites in *C. minor* on an organ basis and during development. Accumulation dynamics of several phytochemicals were analysed using untargeted comparative UPLC-MS and NMR technologies. The UPLC-MS approach utilised herein allowed for the identification of many metabolites, while ^{1}H-NMR provided an absolute quantification of metabolites of different classes. We have reported a novel application of 2D HMBC-NMR to discriminate organs and developmental stages of a plant in the context of its ontogenic variations. This demonstrates the analytical potential of a 2D-NMR platform as an emerging tool for the profiling of complex plant extracts in metabolomics studies, and it presents additional evidence for the complementarity of NMR and UPLC-MS.

The chemical characterisation of complex structures in *C. minor* extracts demonstrates the potential of modern 2D-NMR spectroscopic techniques to speed up the traditional lengthy processes to identify active principles in crude plant extracts, as it can in ideal cases provide enough information to resolve structures even without any purification step,[30] and it speeds up dereplication and identification of known compounds. The emerging NMR metabolomics combined with

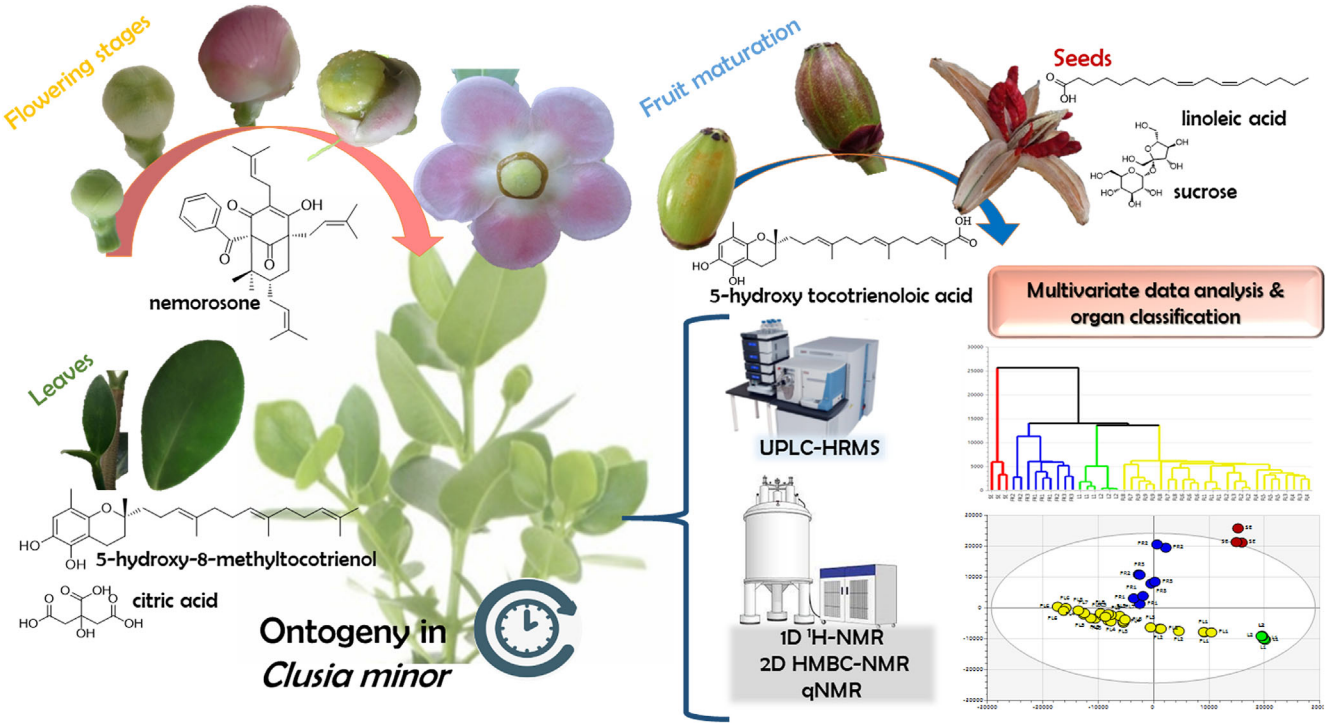

FIGURE 7 *Clusia minor* changes main functional metabolites from citric acid in green parts to bee-collectable nemorosone in flowers and to 5-hydroxy tocotrienoloic acid and energy compounds in seeds. [Colour figure can be viewed at wileyonlinelibrary.com]

modern cheminformatics can indeed help to reduce the gap that has widened in natural product drug discovery, aiding towards identification of active agents especially if coupled to bioassays using regression models such as partial least squares (PLS).[72,73]

Multivariate data analyses coupled to UPLC-MS and 1D/2D-NMR datasets demonstrate variation in secondary metabolism existing among *C. minor* organs, with opening flowers being the richest ones in bioactive polyprenylated benzophenones, particularly nemorosone. The clustering of fruit specimens was mostly attributed to its richness in 5-hydroxy tocotrienoloic acid. In contrast, leaf samples were rich in citric acid and 5-hydroxy-8-methyltocotrienol. Not unexpected, the plant provides to each organ and developmental stage the constituents of prime relevance as major (secondary) metabolite.

Coupling these differential metabolite profile data with gene transcript levels can assist in probing involved genes, biosynthetic pathway analyses, and eventually breeding if targeting increasing levels of that phytochemical.[74,75] Indeed, the correlative analysis of differential metabolic and gene expression profiling *in planta* has proven a powerful approach for the identification of candidate genes and enzymes, particularly for those of natural product metabolism. This aids the identification of the best times for transcriptome analyses and for harvesting certain phytochemicals or enzymes.

The same metabolomics workflow of sample preparation, measurement, and data processing can be adapted easily to other ontogenic studies of secondary metabolite producing plants. The analytical approach developed in this work can also be readily applied for investigating the effect of other factors such as cultivars, storage, harvesting time, or seasonal variation on the secondary metabolite composition of *C. minor* or other plants adding to its potential use as nutraceutical or medicinal plant in the future.

ACKNOWLEDGEMENTS

Clarice Noleto-Dias acknowledges the scholarship received from CNPq. Prof. Mohamed A. Farag acknowledges the funding received by the Alexander von Humboldt Foundation, Germany. We are grateful to Dr. Andrej Frolov and Ms. Annegret Laub for assistance in running the UPLC-MS analysis. Open Access funding enabled and organized by Projekt DEAL.

DATA AVAILABILITY STATEMENT

NMR datasets available at RADAR DOI: 10.22000/1679. Any other data will be made available on request.

ORCID

Mohamed A. Farag https://orcid.org/0000-0001-5139-1863
Josean F. Tavares https://orcid.org/0000-0003-0293-2605

REFERENCES

1. Porzel A, Farag MA, Mülbradt J, Wessjohann LA. Metabolite profiling and fingerprinting of *Hypericum* species: a comparison of MS and NMR metabolomics. *Metabolomics*. 2014;10(4):574-588. doi:10.1007/s11306-013-0609-7
2. Farag MA, Porzel A, Wessjohann LA. Comparative metabolite profiling and fingerprinting of medicinal licorice roots using a multiplex

approach of GC–MS, LC–MS and 1D NMR techniques. *Phytochemistry*. 2012;76:60-72. doi:10.1016/j.phytochem.2011.12.010
3. The Angiosperm Phylogeny Group. An update of the angiosperm phylogeny group classification for the orders and families of flowering plants: APG IV. *Bot J Lin Soc*. 2016;181(1):1-20. doi:10.1111/boj.12385
4. Gustafsson MHG, Winter K, Bittrich V. Diversity, Phylogeny and Classification of Clusia. In: Lüttge U, ed. *Clusia*. Springer; 2007:95-116. doi:10.1007/978-3-540-37243-1_7
5. de Marques EJ, Ferraz CG, dos Santos IBF, et al. Chemical constituents isolated from *Clusia criuva subsp. Criuva* and their chemophenetics significance. *Biochem Syst Ecol*. 2021;97:104293. doi:10.1016/j.bse.2021.104293
6. Stevens PF. Clusiaceae-Guttiferae. In: Kubitzki K, ed. *The families and genera of vascular plants*. Vol.IX. Springer; 2007:48-66. doi:10.1007/978-3-540-32219-1_10
7. Ferraz CG, Ribeiro PR, Mendonça R, Silveira ER, Cruz FG. Novel polyprenylated benzophenone derivatives from *Clusia burle-marxii*. *Fitoterapia*. 2021;149:104760. doi:10.1016/j.fitote.2020.104760
8. Lokvam J, Braddock JF, Reichardt PB, Clausen TP. Two polyisoprenylated benzophenones from the trunk latex of *Clusia grandiflora* (Clusiaceae). *Phytochemistry*. 2000;55(1):29-34. doi:10.1016/S0031-9422(00)00193-X
9. Piccinelli AL, Cuesta-Rubio O, Chica MB, et al. Structural revision of clusianone and 7-epi-clusianone and anti-HIV activity of polyisoprenylated benzophenones. *Tetrahedron*. 2005;61(34):8206-8211. doi:10.1016/j.tet.2005.06.030
10. Gustafson KR, Blunt JW, Munro MHG, et al. The guttiferones, HIV-inhibitory benzophenones from *Symphonia globulifera*, *Garcinia livingstonei*. *Garcinia Ovalifolia and Clusia rosea Tetrahedron*. 1992;48(46):10093-10102. doi:10.1016/S0040-4020(01)89039-6
11. Monzote L, Cuesta-Rubio O, Matheeussen A, Van Assche T, Maes L, Cos P. Antimicrobial evaluation of the polyisoprenylated benzophenones nemorosone and guttiferone A. *Phytother Res*. 2011;25(3):458-462. doi:10.1002/ptr.3401
12. Popolo A, Piccinelli AL, Morello S, et al. Cytotoxic activity of nemorosone in human MCF-7 breast cancer cells. *Can J Physiol Pharmacol*. 2011;89(1):50-57. doi:10.1139/y10-100
13. Cuesta-Rubio O, Frontana-Uribe BA, Ramírez-Apan T, Cárdenas J. Polyisoprenylated benzophenones in cuban propolis; biological activity of nemorosone. *Z Naturforsch C J Biosci*. 2002;57(3–4):372-378. doi:10.1515/znc-2002-3-429
14. Camargo MS, Oliveira MT, Santoni MM, et al. Effects of nemorosone, isolated from the plant *Clusia rosea*, on the cell cycle and gene expression in MCF-7 BUS breast cancer cell lines. *Phytomedicine*. 2015;22(1):153-157. doi:10.1016/j.phymed.2014.11.007
15. Díaz-Carballo D, Gustmann S, Acikelli AH, et al. 7-epi-nemorosone from *Clusia rosea* induces apoptosis, androgen receptor down-regulation and dysregulation of PSA levels in LNCaP prostate carcinoma cells. *Phytomedicine*. 2012;19(14):1298-1306. doi:10.1016/j.phymed.2012.08.004
16. Silva EM, Araújo RM, Freire-Filha LG, et al. Clusiaxanthone and tocotrienol series from *Clusia pernambucensis* and their antileishmanial activity. *J Braz Chem Soc*. 2013;24(8):1314-1321. doi:10.5935/0103-5053.20130166
17. Anholeti MC, De Paiva SR, Figueiredo MR, Kaplan MAC. Chemosystematic aspects of polyisoprenylated benzophenones from the genus *Clusia*. *An Acad Bras Cienc*. 2015;87(1):289-301. doi:10.1590/0001-3765201520140564
18. Farag MA, Wessjohann LA. Cytotoxic effect of commercial Humulus lupulus L. (hop) preparations – in comparison to its metabolomic fingerprint. *J Adv Res*. 2013;4(4):417-421. doi:10.1016/j.jare.2012.07.006
19. Tran HNK, Nguyen VT, Kim JA, et al. Anti-inflammatory activities of compounds from twigs of Morus alba. *Fitoterapia*. 2017;120:17-24. doi:10.1016/j.fitote.2017.05.004
20. Seipold L, Gerlach G, Wessjohann L. A new type of floral oil from *Malpighia coccigera* (Malpighiaceae) and chemical considerations on the eolution of oil flowers. *Chem Biodivers*. 2004;1(10):1519-1528. doi:10.1002/cbdv.200490112
21. Dumri K, Seipold L, Schmidt J, et al. Non-volatile floral oils of *Diascia* spp. (Scrophulariaceae). *Phytochemistry*. 2008;69(6):1372-1383. doi:10.1016/j.phytochem.2007.12.012
22. Schäffler I, Steiner KE, Haid M, et al. Diacetin, a reliable cue and private communication channel in a specialized pollination system. *Sci Rep*. 2015;5(1):12779. doi:10.1038/srep12779
23. Cotrim CA, Weidner A, Strehmel N, et al. A distinct aromatic prenyltransferase associated with the futalosine pathway. *ChemistrySelect*. 2017;2(29):9319-9325. doi:10.1002/slct.201702151
24. Wessjohann LA, Schreckenbach HF, Kaluđerović GN. Enzymatic C-Alkylation of Aromatic Compounds. In: Faber K, Fessner WD, Turner NJ, eds. *Biocatalysis organic synthesis*. Vol.2. Georg Thieme Verlag KG; 2015:177-211. doi:10.1055/sos-SD-215-00096
25. Fobofou SAT, Harmon CR, Lonfouo AHN, Franke K, Wright SM, Wessjohann LA. Prenylated phenyl polyketides and acylphloroglucinols from *Hypericum peplidifolium*. *Phytochemistry*. 2016;124:108-113. doi:10.1016/j.phytochem.2016.02.003
26. Marín RM, De Oca Porto RM, Herrera Paredes ME, et al. GC/MS analysis and bioactive properties of extracts obtained from *Clusia minor* L. *Leaves J Mex Chem Soc*. 2018;62(4):177-188. doi:10.29356/jmcs.v62i4.544
27. Mangas R, Reynaldo G, Dalla Vecchia MT, et al. Gas chromatography/mass spectrometry characterization and antinociceptive effects of the ethanolic extract of the leaves from *Clusia minor* L. *J Pharm Pharmacogn Res*. 2019;7(1):21-30. http://jppres.com/jppres
28. Tomas-Barberan FA, Garcia-Viguera C, Vit-Olivier P, Ferreres F, Tomas-Lorente F. Phytochemical evidence for the botanical origin of tropical propolis from Venezuela. *Phytochemistry*. 1993;34(1):191-196. doi:10.1016/S0031-9422(00)90804-5
29. Mangas Marín R, Bello Alarcón A, Rubio OC, Piccinelli AL, Rastrelli L. Polyprenylated benzophenones derivatives from *Cluisa minor* fruits. *Latin Am J Pharma*. 2008;27(5):762-765.
30. Farag MA, Mahrous EA, Lübken T, Porzel A, Wessjohann L. Classification of commercial cultivars of *Humulus lupulus* L. (hop) by chemometric pixel analysis of two dimensional nuclear magnetic resonance spectra. *Metabolomics*. 2014;10(1):21-32. doi:10.1007/S11306-013-0547-4/METRICS
31. Farag MA, Al-Mahdy DA, Salah El Dine R, et al. Structure-activity relationships of antimicrobial gallic acid derivatives from pomegranate and acacia fruit extracts against potato bacterial wilt pathogen. *Chem Biodivers*. 2015;12(6):955-962. doi:10.1002/cbdv.201400194
32. Gontijo VS, de Souza TC, Rosa IA, et al. Isolation and evaluation of the antioxidant activity of phenolic constituents of the *Garcinia brasiliensis* epicarp. *Food Chem*. 2012;132(3):1230-1235. doi:10.1016/j.foodchem.2011.10.110
33. Fang X, Fu Z, Zhang H, Xu HX, Liang S. Chemical constituents of *Garcinia yunnanensis* and their scavenging activity against DPPH radicals. *Chem Nat Compd*. 2018;54(2):232-234. doi:10.1007/s10600-018-2310-6
34. Deachathai S, Mahabusarakam W, Phongpaichit S, Taylor WC, Zhang YJ, Yang CR. Phenolic compounds from the flowers of *Garcinia dulcis*. *Phytochemistry*. 2005;67(5):464-469. doi:10.1016/j.phytochem.2005.10.016
35. Remali J, Sahidin I, Aizat WM. Xanthone biosynthetic pathway in plants: A review. *Front. Plant Sci*. 2022;13:13. doi:10.3389/fpls.2022.809497
36. Ibrahim SRM, Abdallah HM, El-Halawany AM, Nafady AM, Mohamed GA. Mangostanaxanthone VIII, a new xanthone from *Garcinia mangostana* and its cytotoxic activity. *Nat Prod Res*. 2019;33(2):258-265. doi:10.1080/14786419.2018.1446012

37. Phukhatmuen P, Suthiphasilp V, Rujanapan N, et al. Xanthones from the latex and twig extracts of *Garcinia nigrolineata* planch. Ex T. Anderson (Clusiaceae) and their antidiabetic and cytotoxic activities. *Nat Prod Res*. 2023;37(5):702-712. doi:10.1080/14786419.2022.2086544
38. Oliveira CMA, Porto ALM, Bittrich V, Marsaioli AJ. Two polyisoprenylated benzophenones from the floral resins of three Clusia species. *Phytochemistry*. 1999;50(6):1073-1079. doi:10.1016/S0031-9422(98)00476-2
39. Heinke R, Arnold N, Wessjohann L, Schmidt J. Negative ion tandem mass spectrometry of prenylated fungal metabolites and their derivatives. *Anal Bioanal Chem*. 2013;405(1):177-189. doi:10.1007/s00216-012-6498-1
40. Farag MA, Porzel A, Schmidt J, Wessjohann LA. Metabolite profiling and fingerprinting of commercial cultivars of *Humulus lupulus* L. (hop): a comparison of MS and NMR methods in metabolomics. *Metabolomics*. 2012;8(3):492-507. doi:10.1007/s11306-011-0335-y
41. Monache FD, Monache GD, Gacs-Baitz E. Prenylated benzophenones from *Clusia sandiensis*. *Phytochemistry*. 1991;30(6):2003-2005. doi:10.1016/0031-9422(91)85056-6
42. de Oliveira CMA, Porto AM, Bittrich V, Vencato I, Marsaioli AJ. Floral resins of *Clusia* spp.: chemical composition and biological function. *Tetrahedron Lett*. 1996;37(36):6427-6430. doi:10.1016/0040-4039(96)00656-9
43. Uwamori M, Saito A, Nakada M. Stereoselective total synthesis of nemorosone. *J Org Chem*. 2012;77(11):5098-5107. doi:10.1021/jo300646j
44. Cuesta-Rubio O, Monzote L, Fernández-Acosta R, Pardo-Andreu GL, Rastrelli L. A review of nemorosone: chemistry and biological properties. *Phytochemistry*. 2023;210:210. doi:10.1016/j.phytochem.2023.113674
45. Horvath G, Wessjohann L, Bigirimana J, et al. Accumulation of tocopherols and tocotrienols during seed development of grape (*Vitis vinifera* L. cv. Albert Lavallée). *Plant Physiol Biochem*. 2006;44(11–12):724-731. doi:10.1016/j.plaphy.2006.10.010
46. Horvath G, Wessjohann L, Bigirimana J, et al. Differential distribution of tocopherols and tocotrienols in photosynthetic and non-photosynthetic tissues. *Phytochemistry*. 2006;67(12):1185-1195. doi:10.1016/j.phytochem.2006.04.004
47. Mitei YC, Ngila JC, Yeboah SO, Wessjohann L, Schmidt J. Profiling of phytosterols, tocopherols and tocotrienols in selected seed oils from Botswana by GC–MS and HPLC. *J Am Oil Chem Soc*. 2009;86(7):617-625. doi:10.1007/s11746-009-1384-5
48. Teixeira JSR, Da L, Guedes S, Cruz FG. A new biphenyl from Clusia Melchiorii and a new Tocotrienol from C. *Obdeltifolia*. 2006;17(4):812-815. doi:10.1590/S0103-50532006000400027
49. Ribeiro PR, Ferraz CG, Guedes MLS, Martins D, Cruz FG. A new biphenyl and antimicrobial activity of extracts and compounds from *Clusia burlemarxii*. *Fitoterapia*. 2011;82(8):1237-1240. doi:10.1016/j.fitote.2011.08.012
50. Bartolini D, De Franco F, Torquato P, et al. Garcinoic acid is a natural and selective agonist of pregnane X receptor. *J Med Chem*. 2020;63(7):3701-3712. doi:10.1021/acs.jmedchem.0c00012
51. Kluge S, Schubert M, Schmölz L, Birringer M, Wallert M, Lorkowski S. Garcinoic acid: A promising bioactive natural product for better understanding the physiological functions of tocopherol metabolites. In: *Studies in natural products chemistry*. Vol.51; 2016:435-481. doi:10.1016/B978-0-444-63932-5.00009-7
52. Tchimene MK, Anaga AO, Ugwoke CEC, et al. Anti-diabetic profile of extract, kolaviron, biflavonoids and garcinoic acid from *Garcinia kola* seeds. *Int J Curr Microbiol Appl Sci*. 2016;5(2):317-322. doi:10.20546/ijcmas.2016.502.036
53. Maloney DJ, Hecht SM. A Stereocontrolled synthesis of δ-*trans*-Tocotrienoloic acid. *Org Lett*. 2005;7(19):4297-4300. doi:10.1021/ol051849t
54. Wang X, Li R, Liu X, et al. Study on characteristics of biflavanones distribution in *Garcinia kola* seeds and identification of compounds in gum resin exuded from fresh slices. *J Pharm Biomed Anal*. 2020;190:113512. doi:10.1016/j.jpba.2020.113512
55. Sangsopha W, Schevenels FT, Lekphrom R, Kanokmedhakul S. A new tocotrienol from the roots and branches of *Allophylus cobbe* (L.) Raeusch (Sapindaceae). *Nat Prod Res*. 2020;34(7):988-994. doi:10.1080/14786419.2018.1547298
56. Noleto-Dias C, de Picoli EAT, Porzel A, Wessjohann LA, Tavares JF, Farag MA. Metabolomics characterizes early metabolic changes and markers of tolerant *Eucalyptus* ssp. clones against drought stress. *Phytochemistry*. 2023;212:113715. doi:10.1016/j.phytochem.2023.113715
57. Malz F. Quantitative NMR in the solution state NMR. In: Holzgrabe U, Wawer I, Diehl B, eds. *NMR spectroscopy in pharmaceutical analysis*. 1st ed. Elsevier Ltd; 2008:43-62. doi:10.1016/B978-0-444-53173-5.00002-0
58. Mahgoub YA, Shawky E, Ghareeb DA, Darwish FA, El Sebakhy NA, El-Hawiet AM. UPLC-MS/MS multivariate data analysis reveals phenological growth stages affect silymarin bioactive components of the different organs of two *Silybum marianum* genotypes. *Microchem J*. 2023;187:108436. doi:10.1016/j.microc.2023.108436
59. Nelson AS, Whitehead SR. Fruit secondary metabolites shape seed dispersal effectiveness. *Trends Ecol Evol*. 2021;36(12):1113-1123. doi:10.1016/J.TREE.2021.08.005
60. Pachon P, Winter K, Lasso E. Updating the occurrence of crassulacean acid metabolism (CAM) in the genus *Clusia* through carbon isotope analysis of species from Colombia. *Photosynthetica*. 2022;60(2):304-322. doi:10.32615/ps.2022.018
61. De Mattos EA, Herzog1 B, Lü U. Chlorophyll fluorescence during CAM-phases in Clusia Minor L. under drought. *Stress*. 1999. https://academic.oup.com/jxb/article/50/331/253/563007;50:261. doi:10.1093/jexbot/50.331.253
62. Yang B, Zhong Z, Wang T, et al. Integrative omics of *Lonicera japonica* Thunb. Flower development unravels molecular changes regulating secondary metabolites. *J Proteomics*. 2019;208:103470. doi:10.1016/j.jprot.2019.103470
63. Dias CN, de Picoli EAT, de Souza GA, et al. Phenolics metabolism provides a tool for screening drought tolerant *Eucalyptus grandis* hybrids. *Aust J Crop Sci*. 2017;11(8):1016-1024. https://www.cropj.com/picoli_11_8_2017_1016_1024.pdf
64. Önder S, Tonguç M, Erbaş S, Önder D, Mutlucan M. Investigation of phenological, primary and secondary metabolites changes during flower developmental of *Rosa damascena*. *Plant Physiol Biochem*. 2022;192:20-34. doi:10.1016/J.PLAPHY.2022.09.032
65. Tsafack Nguemo RB, Njouendou AJ, Simo Mpetga JD, et al. Antimicrobial activities of chemical constituents from the flowers of *Hypericum lanceolatum* lam. *(Hypericaceae) IJAMBR*. 2020;8:66-72. doi:10.33500/ijambr.2020.08.007
66. Szewczyk K, Chojnacka A, Górnicka M. Tocopherols and Tocotrienols—Bioactive Dietary Compounds; What Is Certain, What Is Doubt? *Int J Mol Sci*. 2021;22(12):6222. doi:10.3390/IJMS22126222
67. Matringe M, Ksas B, Rey P, Havaux M. Tocotrienols, the unsaturated forms of vitamin E, can function as antioxidants and lipid protectors in tobacco leaves. *Plant Physiol*. 2008;147(2):764-778. doi:10.1104/PP.108.117614
68. De La Pascua DR, Smith-Winterscheidt C, Dowell JA, Goolsby EW, Mason CM. Evolutionary trade-offs in the chemical defense of floral and fruit tissues across genus *Cornus*. *Am J Bot*. 2020;107(9):1260-1273. doi:10.1002/ajb2.1540
69. Herms DA, Mattson WJ. The dilemma of plants: to grow or defend. *Source: Q Rev Biol*. 1992;67(3):283-335. https://about.jstor.org/terms. doi:10.1086/417659
70. Yuk J, McKelvie JR, Simpson MJ, Spraul M, Simpson AJ. Comparison of 1-D and 2-D NMR techniques for screening earthworm responses

to sub-lethal endosulfan exposure. *Environ Chem*. 2010;7(6):524. doi:10.1071/EN10084

71. Farag MA, Porzel A, Al-Hammady MA, et al. Soft corals biodiversity in the Egyptian red sea: a comparative MS and NMR metabolomics approach of wild and aquarium grown species. *J Proteome Res*. 2016;15(4):1274-1287. doi:10.1021/acs.jproteome.6b00002
72. Farag MA, Aboul Naser AF, Zayed A, Sharaf El-Dine MG. Comparative insights into four major legume sprouts efficacies for diabetes management and its complications: untargeted versus targeted NMR biochemometrics approach. *Metabolites*. 2022;13(1):63. doi:10.3390/metabo13010063
73. Degenhardt A, Wittlake R, Seilwind S, et al. Quantification of important flavor compounds in beef stocks and correlation to sensory results by "Reverse Metabolomics.". In: *Flavour Science*. Elsevier; 2014:15-19. doi:10.1016/B978-0-12-398549-1.00003-9
74. Burgos-Toro A, Dippe M, Felipe Vásquez A, Pierschel E, Aloisius Wessjohann L, Fernández-Niño M. Multi- *omics* data mining: A novel tool for BioBrick design. In: *Synthetic Genomics - From BioBricks to Synthetic Genomes*. IntechOpen; 2022. doi:10.5772/intechopen.101351
75. Feiner A, Pitra N, Matthews P, Pillen K, Wessjohann LA, Riewe D. Downy mildew resistance is genetically mediated by prophylactic production of phenylpropanoids in hop. *Plant Cell Environ*. 2021;44(1):323-338. doi:10.1111/pce.13906

SUPPORTING INFORMATION

Additional supporting information can be found online in the Supporting Information section at the end of this article.

How to cite this article: Noleto-Dias C, Farag MA, Porzel A, Tavares JF, Wessjohann LA. A multiplex approach of MS, 1D-, and 2D-NMR metabolomics in plant ontogeny: A case study on *Clusia minor* L. organs (leaf, flower, fruit, and seed). *Phytochemical Analysis*. 2023;1-24. doi:10.1002/pca.3300